CHARLES UNIVERSITY IN PRAGUE
Faculty of Mathematics and Physics

DOCTORAL THESIS

2010 JAN ČERMÁK

CHARLES UNIVERSITY IN PRAGUE
FACULTY OF MATHEMATICS AND PHYSICS

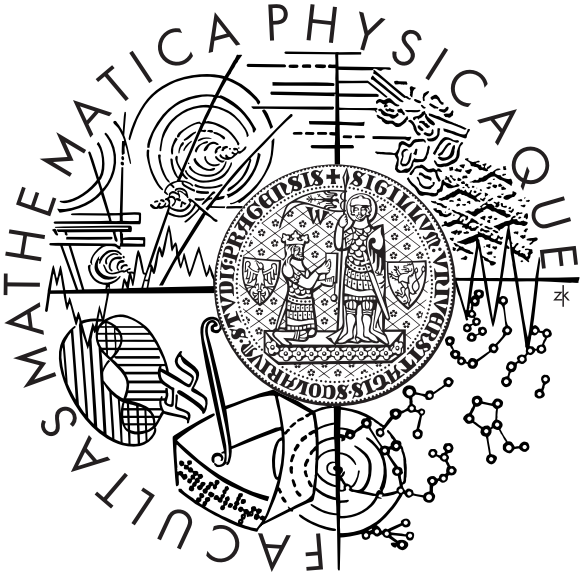

DOCTORAL THESIS

Semiconductor - organic interface at nanoscale

by

RNDr. Jan Čermák

Prague, 2010

A doctoral thesis submitted in partial satisfaction of the requirements for the post-graduate degree of Charles University, Prague, Czech Republic

Semiconductor - organic interface at nanoscale

Supervisor:

RNDr. Antonín Fejfar, CSc.
Institute of Physics,
Academy of Sciences of the Czech Republic, v.v.i.

Consultants:

RNDr. Bohuslav Rezek, Ph.D.
Institute of Physics, Academy of Sciences of the Czech Republic, v.v.i.

RNDr. Věra Cimrová, CSc.
Institute of Macromolecular Chemistry,
Academy of Sciences of the Czech Republic, v.v.i.

Prague, June 2010

Acknowledgements

I would like to thank RNDr. Antonín Fejfar, CSc., my supervisor, for offering me the opportunity to spend my post-graduate studies under his leadership and for supporting me with comfortable research conditions. Many thanks belong particularly to RNDr. Bohuslav Rezek, Ph.D., my consultant - specialist, who spent a lot of time not only teaching me various experimental techniques but also giving me a general insight to what responsible, reliable and respectful scientific research necessarily should include. I would also like to thank RNDr. Věra Cimrová, CSc., my second consultant - specialist, for supporting me with experimental equipment as well as highly important inputs on the chemical parts of the work.

My sincere thanks belong to Ing. Tomáš Mates, Ph.D., who first introduced me to the atomic force microscopy. RNDr. Martin Ledinský, Ph.D., has also to be mentioned here as without his micro-Raman analysis most of the work would miss the crucial information about chemical composition. Ing. Alexander Kromka, Ph.D., is another person who beneficially supported me by his complex knowledge of diamond technology. I need to express my thanks to Ing. Vlastimil Jurka for teaching me the basics of optical lithography and RNDr. Zdeněk Výborný, CSc., for allowing me to use the clean-room laboratory. I also would like to acknowledge RNDr. Pavel Hubík, CSc., and RNDr. Jiří J. Mareš, CSc., for the Hall mobility experiment and related discussions.

My thanks also belong to the whole team at the Department of Thin Films and Nanostructures at the Institute of Physics, Academy of Sciences of the Czech Republic, v.v.i. for creating a friendly atmosphere during my post-graduate research. Special thanks should be expressed to the head of the department, RNDr. Jan Kočka, DrSc., for his open-minded approach to the novel topics of research at the department. Also the careful help of Petra Šnajdrová during my stay at the Institute of Physics should be highlighted.

This research has been supported by the following grants: Ministry of Education, Youth and Sports of the Czech Republic (grants No. 1M06031, AV0Z10100521, LC06040, LC510), the Grant Agency of the Czech Republic (grant No. 202/09/H041) and of the Academy of Sciences of the Czech Republic (project No. KAN400100701 and the Fellowship J.E. Purkyně).

The last, but the most cordial thanks belong to my family, starting with my wife Kateřina together with our recently born daughter Magdaléna and ending with my parents, for preparing a very thoughtful environment to my post-graduate studies.

Doc. RNDr. Jaromír Fähnrich, CSc., and Mgr. Jan Fähnrich, CSc., also deserve to be mentioned gratefully as the discussions with them during my childhood and adolescence started my interest in science and also helped me to discover the charm of scientific research.

Abstract

Organic materials are promising for many fields of applications, especially for photovoltaics due to relatively low processing costs and large versatility. The photovoltaic efficiency of organic photovoltaic cells is still too low for wider industrial fabrication. One of the mostly studied type of organic photovoltaic cells is the so-called bulk-heterojunction structure. It is a thin film (typical thickness 100 nm) made of a mixture of two organic materials forming interpenetrating network. It is obvious, that the electronic properties of such devices are governed by microscopic ordering. Therefore characterizing and understanding their microscopic structural, chemical, electronic as well as opto-electronic properties is important for their further improvement. Scanning probe microscopy is a powerful tool for such a characterization as apart from visualizing topography, it can also study electronic and opto-electronic properties with high spatial resolution.

The thesis starts with application of various scanning probe microscopic techniques (atomic force microscopy, Kelvin force microscopy, current-sensing atomic force microscopy and mapping of micro-Raman scattering) on organic blend thin films. The correlation of these techniques applied on an organic photovoltaic cell helped us to reveal the reason for low photovoltaic efficiency in spite of efficient photoluminescence quenching. We also demonstrate that Kelvin force microscopy performed under repeated illumination switching on and off can resolve different opto-electronic properties of various blend thin films even when their topography and surface potential images look similar.

Next part of the thesis deals with a system made of a diamond and an organic dye (polypyrrole). Such a system is promising for various types of novel opto-electronic as well as biological or chemical sensors. From the opto-electronic point of view this system turned out to be similar to the fully organic bulk-heterojunction photovoltaic cells. We proved that polypyrrole is covalently bound to diamond surface after electrochemical synthesis. Based on the advanced AFM characterization novel opto-electronic properties of this system were revealed. A model of charge transfer from polypyrrole to diamond under illumination via interfacial trap states was proposed. The model is supported by both indirect (loss of diamond surface conductivity, surface photovoltage effect) and direct (Hall mobility measurement) experimental results.

Abstrakt

Organické materiály jsou potenciálně výhodně využitelné v mnoha oborech, zejména ve fotovoltaice, protože mohou mít různé volitelné vlastnosti a jejich výroba je relativně levná. Průmyslové výrobě organických fotovoltaických článků ale zatím brání jejich nízká fotovoltaická účinnost. Jedním z nejvíce studovaných konceptů organického fotovoltaického článku je takzvaný objemový heteropřechod. Jedná se o tenkou vrstvu (typická tloušťka 100 nm) směsi dvou organických látek tvořících navzájem propletenou síť. Je zřejmé, že elektronické chování takových struktur je výrazně ovlivňováno jejich mikroskopickým uspořádáním. Pro vylepšení jejich vlastností je tedy nutné studovat a rozumět jejich mikroskopickým strukturním, chemickým, elektronickým a také opto-elektronickým vlastnostem. Pro takovou charakterizaci se hodí metody skenovací sondové mikroskopie, protože kromě topografie dokáží zachytit i elektronické a opto-elektronické vlastnosti s vysokým prostorovým rozlišením.

První část této dizertační práce pojednává o charakterizaci směsných organických tenkých vrstev několika různými skenovacími mikroskopickými metodami (mikroskopie atomárních sil, mikroskopie Kelvinovskou sondou, mikroskopie atomárních sil s detekcí elektrického proudu a mapování mikro-Ramanovským spektrometrem). Korelací výsledků těchto technik jsme objevili příčinu nízké fotovoltaické účinnosti studované heterostruktury i přes pozorované účinné zhášení fotoluminiscence. Dále ukážeme, že mikroskopie Kelvinovskou sondou dokáže odlišit různé opto-elektronické chování organických tenkých vrstev, i když jejich topografické obrázky a obrázky povrchového potenciálu vypadají stejně.

Další část se věnuje opto-elektronickým vlastnostem systému tvořeného diamantem a organickým barvivem (polypyrrol). Takový systém by byl velmi vhodný pro použití v nových typech biologických nebo chemických senzorů. Ukázalo se, že opto-elektronické jevy v takovém systému jsou velmi podobné těm ve slunečních článcích tvořených objemovým heteropřechodem. Prokázali jsme, že při elektrochemické syntéze polypyrrolu na diamantu se mezi těmito materiály vytvoří kovalentní vazba. Na základě pokročilé charakterizace metodami mikroskopie atomárních sil jsme objevili nové opto-elektronické jevy. Sestavili jsme model přenosu náboje z polypyrrolu do diamantu přes pasťové stavy na rozhraní při osvětlení. Tento model jsme podpořili jak nepřímými (ztráta povrchové vodivosti diamantu, efekt povrchového fotonapětí), tak i přímými (měření Hallovy pohyblivosti nosičů náboje) experimentálními výsledky.

Contents

Chapter 1

INTRODUCTION

When Thomas Seebeck observed semiconducting properties of lead sulfide in 1823 he was not aware that in one and a half century semiconductor-based electronic devices would accompany people in their everyday lives. The invention of the transistor by William Shockley, John Bardeen and Walter Brattain in 1947 was the starting point for the fabrication of the first integrated circuit by Jack Kilby in 1958 which allowed further miniaturization of electronic devices. Nowadays the semiconductor-based electronic devices can be found in many areas including, for example, medicine, car industry or computer science. In 1954 Daryl M. Chapin, Calvin S. Fuller and Gerald L. Pearson demonstrated that semiconductors (silicon in this case) are suitable also for the conversion of sunlight into electric energy.

All the above applications are commonly based on inorganic semiconductors (e.g. silicon or germanium) and thus face the problem of high-cost industrial processes (high-vacuum technology, clean rooms or high purity source materials). A possible way to reduce costs is the use of organic materials with semiconducting or conducting properties. Although the first report on conductivity of doped polypyrrole was published in 1963 [1], the breakthrough is attributed to the work on doped polyacetylene from 1977 by A.J. Heeger, H. Shirakawa and A.G. MacDiarmid [2], for which they were awarded the Nobel prize in 2000. Since then organic semiconductors have followed similar scientific evolution as inorganic ones (all-polymer field effect transistor in 1994 [3], organic integrated circuit by the Philips company (1998)...) until recent days, which have seen organic displays in cell phones and the start of industrial production of organic photovoltaic cells by the first commercial company (Konarka Technologies GmBH).

As organic materials are commonly disordered systems and are often used in a mixture of several components, their properties are governed by microscopic order-

ing. Therefore characterizing and understanding of microscopic structural, chemical, electronic as well as opto-electronic properties is important for further improvement and wider industrial application. Among many microscopical techniques, scanning probe microscopy (SPM) is a powerful tool for such characterizations as, apart from visualizing topography, it can also be used for electronic and optoelectronic properties study and mechanical modification with high spatial resolution. Various SPM techniques are described in detail in *Chapter Two* together with the basic principles of Raman scattering, which is capable of chemical composition determination.

A typical example of a system where microscopic ordering plays a key role is the so-called bulk-heterojunction photovoltaic cell. *Chapter Three* deals with the correlation of AFM topography, Kelvin force microscopy (KFM), current-sensing AFM and micro-Raman mapping, which revealed the influence of microscopic ordering on macroscopic properties (photovoltaic power conversion efficiency). The chapter also demonstrates that bulk-heterojunction organic layer opto-electronic properties and their kinetics under illumination can be analyzed via changes in surface potential by KFM.

In *Chapter Four* we apply the knowledge obtained from microscopy on blend organic thin films to a system consisting of organic dye (polypyrrole) and diamond, which is a promising model system of the novel family of nanoscaled biological and chemical sensors. We demonstrate that SPM techniques can also study processes at the polypyrrole-diamond interface, which is not directly touched by the AFM probe (e.g. is hidden under the polypyrrole film). Based on the experimental data we suggested a model of charge transfer from polypyrrole to diamond.

Chapter Five summarizes the results and provides broader perspectives of the present work.

1.1 Organic conducting and semiconducting materials

Organic materials are commonly highly electrically insulating. There are two basic approaches how to make them conductive: either by incorporating carbon particles (method widely used for plastic tools which need to be prevented from electrostatic charging) or to fabricate a material that is conductive itself. One group of such self-conductive materials are conjugated polymers. The conjugated system (single and double bonds are alternating regularly) makes the organic material capable of electrical charge transport due to the delocalized density of electronic states along

the chain. If there are free charge carriers present (e.g. due to internal or external dopant or illumination) the polymers behave in many aspects as ordinary conductors or semiconductors. Yet, there are also differences.

1.2 Organic photovoltaic cells

1.2.1 Fully organic donor-acceptor systems

Photovoltaic effect in organic materials is different from inorganic ones. The binding energy between photo-excited electron-hole pair is strong due to the low dielectric constant, typically in the order of 1 eV. Therefore, the excitons are not dissociated by thermal energy, which is approximately 26 meV at room temperature. A new energy source is needed, for example the potential slope at the interface with a (metal) electrode. This process is not very efficient in a PV cell consisting of a single material, as the exciton diffusion length in organic materials is typically around 10 nm [4]. This is much shorter than the total film thickness needed for efficient light harvesting (100-200 nm). As a result, the majority of photo-generated excitons (which are not generated within the 10 nm distance from an electrode) recombine uselessly. Typical photovoltaic power conversion efficiencies of such devices were around 0.1% [5, 6].

Slight enhancement has been achieved by introducing a layer of a second organic material, resulting in the so called double-layer cell (Fig. 1.1a). By proper choice of the energy levels (HOMO - highest occupied molecular level and LUMO - lowest unoccupied molecular level) of the materials a charge separation with high efficiency can be achieved. However, in this concept the problem of short exciton diffusion length is still not solved.

Significant improvement came with the bulk-heterojunction design [7]. The basic principle of such a design is similar to the double-layer cell, but in the bulk-

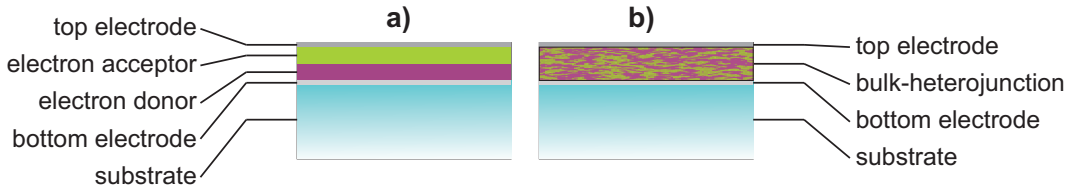

Figure 1.1: *a) double layer organic photovoltaic cell; b) bulk-heterojunction organic photovoltaic cell.*

heterojunction design both materials (donor and acceptor) are prepared as a microscopic interpenetrating network (Fig. 1.1b). Therefore, wherever the excitons are generated, an interface with the other material is always closer than the exciton diffusion length (in an ideal case). The remaining problem is to ensure efficient charge carrier transport to electrodes. So far the best reported PV efficiency is reaching 6% [8, 9]. There are several general approaches which can increase the efficiency:

- morphology control
- efficiency of light harvesting
- match of absorption spectrum with solar spectrum
- fabrication of tandem cells

Morphology is the crucial factor for the organic bulk-heterojunction PV cell properties. If the domains of donor and acceptor materials are too large, the advantage of efficient exciton dissociation is lost, as the interfaces are too far. If the domains are too small, it is difficult to find a continuous path for charge carriers from the bulk to the electrodes. Therefore, the ideal morphology of the interpenetrating network is different for particular materials (according to their opto-electronic properties). However, even if the ideal morphology is proposed theoretically, it may not be easy to achieve in real devices. There are so far two ways how to control the bulk-heterojunction morphology: thermal annealing and additives.

Thermal annealing is known to improve the PV efficiency by a factor of 3-5 [10]. Based on the AFM characterization it is accompanied also by changes in morphology. The effect of annealing is dependent on the annealing temperature. By increasing temperature, the efficiency is increasing as well. This trend is limited by a threshold temperature (e.g. 150-180°C for the P3HT:PCBM system), at which the chemical decomposing of the organic materials and negative morphology changes start.

The morphology of the film can be controlled directly during the preparation process (contrary to thermal annealing, which is applied after the thin film preparation) by adding specific additives to the original solution. For example, such a technique improved the PV power conversion efficiency of a cell made of a conjugated polymer and fullerene derivative by adding alkene dithiols from 2.8% to 5.5% [11].

Cell efficiency can be also increased by an efficient use of light. In a standard organic PV cell design the light intensity in the volume is decreasing due to optical absorption. As a result, the area near the back electrode is almost in the dark and

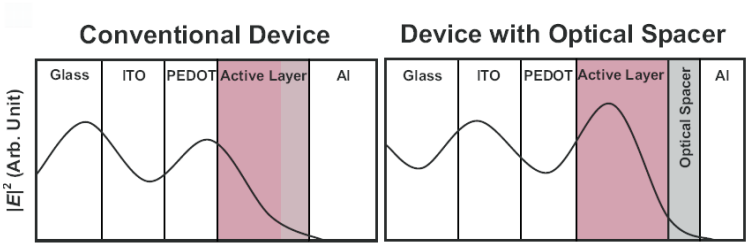

Figure 1.2: *Light intensity in the PV cell without and with an optical spacer (reproduced from the reference [12].*

its contribution to the external electric current is minimal. The light intensity in the active area can be increased via interference effects by introducing an additional reflecting layer - so called optical spacer (Fig. 1.2). However, it is not easy to find a proper material for such an optical spacer. Apart from optical transparency (in the visible spectral region) it has to be a good electron acceptor and conductor and its work function must be properly matched with energy levels of the electron accepting electrode as well as the active material. Titanium dioxide is an example of such a material and was successfully applied in the P3HT:PCBM device. The optical spacer increased the PV power conversion efficiency from 2.3% to 5.0% [12].

Another limiting factor is the mismatch between the absorption spectrum of the devices and the solar spectra. Organics are commonly large bandgap materials and therefore are capable of absorbing the high-energetic part of the solar light. It is proposed that by using materials with lower bandgap the efficiency should be increased. Several attempts have been done using polythiophene-benzothiadiazole or polyfluorene-benzothiadiazole copolymers (HOMO-LUMO gap 1.5-1.9 eV) as electron donors with PCBM (electron acceptor). However, resulting power conversion efficiency was below 4% due to the low fill factor [13].

The efficiency of solar cells may also be increased by the use of "multiple" cells in one system - tandem cells, which are well known from the inorganic PV cell development. The top cell is made of a wide band gap material and absorbs high energetic light, while low energetic light passes through to the bottom cell. This is made of a small band gap material and absorbs the rest of the light. In an ideal case the resulting output is the sum of the outputs of the single standing cells. However, especially in the case of organic PV cells, there is a huge problem in fabrication. Organics are commonly processed by wet techniques and therefore fabrication of one cell on another is difficult, as the further application of a solvent may damage the existing bottom cell.

The above factors represent several already proven and independent technological steps to improve organic PV cells' properties. Each of the steps can multiply the efficiency, so an organic PV cell efficiency higher than 20% is theoretically achievable. The problem lies in the fact that it is extremely difficult to combine all the features in one device. This motivated us to perform the experiments presented in the thesis with the view to reveal a better insight into the basic electronic as well as optoelectronic properties of not only organic PV cells, but of organics combined with inorganic materials as well.

1.2.2 Organic - inorganic systems

For a long time electronics was a domain of inorganic materials. Even though electronic behavior of organic materials has been known for several decades, their applications are still limited. So far the research and development of organic and inorganic electronics has been strictly divided, although their combination might be fruitful. An example of promising organic-inorganic (hybrid) systems is the dye-sensitized PV cell. In this so called Grätzel cell [14], a photoexcited organic dye gives electrons to the electrode via porous inorganic TiO_2. The missing electron is returned from the surrounding electrolyte, which restores the original state at the counter electrode. Although the photovoltaic power conversion of this type of photovoltaic cells is relatively high (10-12%), their wider application is limited by the need of an electrolyte, which is commonly in liquid form.

1.2.3 Characterization

Organic-based electronic as well as optoelectronic devices are commonly made of several compounds and their mutual electronic cooperation at microscale is of key importance for the device properties. Therefore, the revealing and understanding of microscopic structural, chemical, electronic and optoelectronic properties is crucial for their further improvements. Such universal demands may be fulfilled by techniques based on local probe scanning. In our research we focused primarily on the use of atomic force microscopy (AFM), as the sharp tip in the microscope can detect both morphologic and electronic information with high lateral resolution. Additional spatially resolved chemical information is obtained by micro-Raman mapping, where the focused laser beam plays the role of the scanning probe. The following chapter provides a brief description of these local probe techniques.

Chapter 2

EXPERIMENTAL TECHNIQUES

2.1 Scanning probe microscopy

The resolution of optical microscopy is restricted by the diffraction limits to approximately 1 μm for visible light. Higher resolution may be achieved by a system operating with a light with smaller wavelengths. However, enhancing optical microscopy by moving to UV or even X-ray wavelengths is not the proper way, as appropriate optical components are difficult to fabricate. Short wavelength electromagnetic field may also damage the studied object. These limitations were partially solved by the use of the electron beam. However, the need of vacuum, high voltage, at least some sample conductivity, and many additional equipment items make this technique more complicated.

To overcome some of the above limits, a completely new approach has to be applied. It is based on scanning by a local probe on the sample surface. The idea itself is relatively old, but the problem was how to detect movements of the probe with sufficient precision. The breakthrough came with the construction of the scanning tunneling microscope (STM) in 1981 [15] where the sample-probe distance is detected by a tunneling current. This invention was awarded the Nobel prize merely five years (1986) later and gave rise to a large family of scanning probe microscopies. One of them is the atomic force microscopy (AFM) [16]. In contrast to STM, in AFM the probe position is controlled via reflection of a laser beam and thus it allows also the study of electrically insulating materials.

2.1.1 Atomic force microscopy

The most important part of an atomic force microscope is a sharp tip attached to a flexible cantilever. To obtain an image of the surface topography the tip is brought into close vicinity of the studied surface. The tip-sample contact is governed by several types of short-range and long-range interactions. Van der Waals interaction and ionic repulsion are the most important of them. In general, the overall interaction is commonly described by the Lennard-Jones potential:

$$V(r) = A\left[\left(\frac{B}{r}\right)^{12} - \left(\frac{B}{r}\right)^{6}\right] \tag{2.1}$$

where the constants A and B characterize the particular system and r is distance. Schematic visualization of the potential is in Fig. 2.1.

When the AFM tip is brought into contact with the sample or its near vicinity (in nanometer range) the cantilever bends according to the tip-sample interaction. These deflections are detected by a reflected laser beam. The mechanical deflection of the cantilever is then used to evaluate the morphology of the sample surface.

There are many types of AFM probes. Their most important property is sharpness, as it gives the lateral resolution. Sharpness is commonly described by the curvature radius and typical values of commercially available probes are 10-20 nm. The stiffness of the cantilever carrying the tip defines the preferred scanning regime. The soft probes are more suitable for contact mode scanning, hard probes work better at tapping mode or lithography. For electrical modes the crucial property is electric conductivity, which is achieved either by doping the bulk material (typically silicon) or by coating the probe by metals. However, coating always partially degrades the probe,

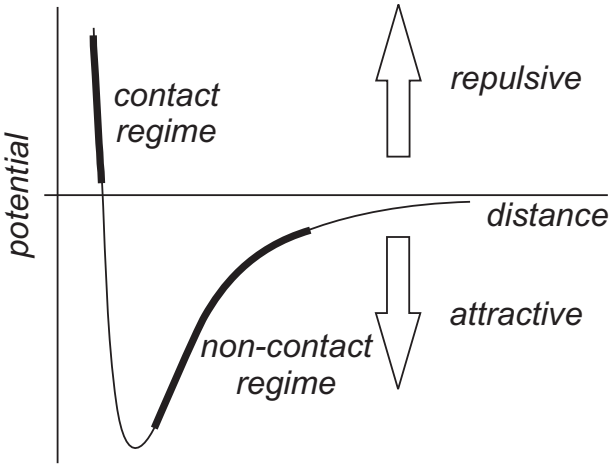

Figure 2.1: *Schematic visualization of the Lennard-Jones potential with emphasized AFM operation regions.*

as it decreases the sharpness and if it is not fabricated properly, it may delaminate when the probe scans the surface. This may lead to diverse artifacts.

Two basic scanning regimes are generally defined, depending on the tip-sample distance: contact and non-contact modes. When the AFM tip is placed into physical contact with the surface, the interaction between them is repulsive - contact mode. When there is a small gap between the tip and sample, the cantilever bending is controlled by attractive interaction - non-contact mode. There is also a widely used third option where the tip is oscillating between both the attractive and repulsive part of the interaction. This regime is called semicontact or tapping mode.

Contact mode

The simplest scanning regime is the contact mode scanning. In this mode, the tip is placed into contact with the surface and is dragged on the surface (Fig. 2.2a). The topography variations then cause the bending of the cantilever, which is used to visualize the surface topography. Basically, there are two types of this regime. In the constant height regime, the chip with the cantilever is held at the same z-position and the topography is detected by the changes of bending of the cantilever. In the constant force regime, the z-position is dynamically adjusted to keep the constant bending of the cantilever (which is equivalent to the contact force). Usually, the constant force is used for general scanning, the constant height is suitable for the scanning of small areas with small z-variations and for samples which is hard enough to resist scratching by the AFM tip, as the contact force is dependent on the AFM tip bending.

Non-contact mode

More gentle to the sample is the non-contact regime. The tip is kept in a distance at which the attractive force is dominating (Fig. 2.2b). As the attractive forces are weak, the simple detection of cantilever bending would not be precise enough. There-

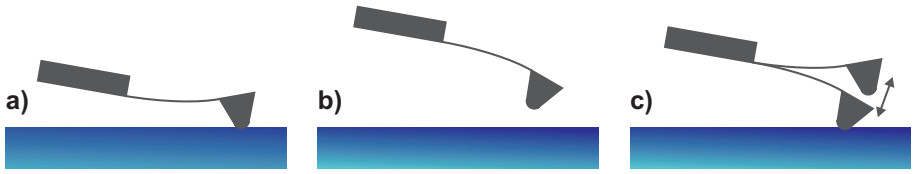

Figure 2.2: *AFM regimes: a) contact, b) non-contact, c) semicontact.*

fore in the non-contact regime the tip is commonly oscillating at low amplitudes (several nm) and the topography is deduced from either amplitude or frequency changes. This regime may be sometimes misleading, especially in air, when the surface of the sample is covered by an adsorbed water layer and the quality factor of the cantilever resonance is low compared to vacuum. In this case the microscope characterizes the surface of the water layer instead of the sample.

Semicontact mode

The probability of unwanted modification or misleading information can be reasonably reduced by the semicontact regime (sometimes called tapping-mode). The tip is not in a permanent direct contact with the surface, but the cantilever is oscillating (usually at its resonant frequency at higher amplitudes 10-100 nm), so that at the top position it is several tens of nanometers far away from the surface, whereas at the bottom position it is slightly touching the surface (Fig. 2.2c). The topography is then derived from the changes of the oscillating amplitude, which is changing according to the tip-sample interaction at the bottom position.

2.1.2 Kelvin force microscopy (KFM)

Apart from the basic regimes measuring morphology, AFM is also capable of detecting other (electronic or mechanical) material properties. One of such advanced regimes is Kelvin force microscopy (KFM, sometimes called Kelvin probe microscopy or Kelvin probe force microscopy). It is based on the standard Kelvin method. When two materials with different work functions (AFM tip and sample, in the case of KFM) are electrically connected (e.g. by external wire) electrons from the lower

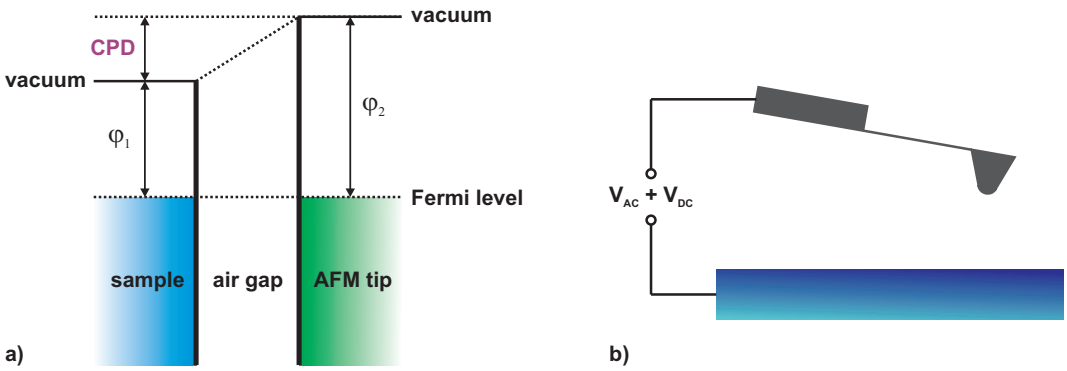

Figure 2.3: *Kelvin force microscopy: a) energy scheme, b) instrumental setup.*

work function material flow to the higher work function material to equalize the Fermi level in the system.

The work function of the studied surface can be estimated by the comparison of the contact potentials of the tip and the sample. This can be done by applying an AC voltage between the sample and the AFM tip, when the tip is at a certain distance from the surface. As their surface potentials are different, this AC voltage creates an electrostatic force that makes the tip oscillate. These oscillations can be minimized to zero by applying an additional DC voltage (found by a feedback loop) to compensate the contact potential difference. The value of the added DC bias voltage represents the value of the contact potential difference. Therefore, if the tip surface potential is calibrated, the absolute values of the surface potential (and then the work function) can be obtained.

2.1.3 Current-sensing atomic force microscopy (CS-AFM)

The contact mode scanning provides a mechanical tip-sample contact, which can be used also for the characterization of microscopic conductivity. When the tip is in contact with the studied surface, a bias voltage is applied between the sample and the AFM tip and the induced electric current is dependent on the conductivity at the position of the tip. As a result, maps of both topography and local conductivity are obtained at once.

Due to the high point-probe contact resistivity (more than 10 GΩ), the detected current is very low (usually fA-nA). It is a tunneling current, similar to the one used in STM for the detection of topography, but in this case, the topography is detected

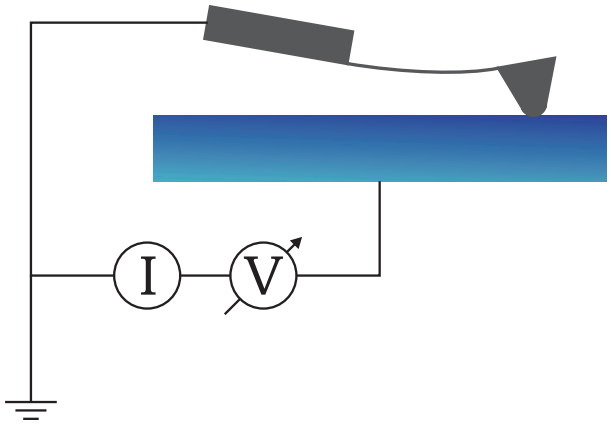

Figure 2.4: *Current-sensing atomic force microscopy.*

by a reflection of a laser beam and the tunneling current brings additional information about electric conductivity.

This mode is usually used to study electronic properties of thin films deposited on a conductive material (bottom electrode), e.g. silicon photovoltaic cells.

Applying this mode on organic materials is rather difficult due to the need of a contact regime. The soft organic materials can be easily damaged by the sharp AFM tip (radius typically 10-30 nm).

2.1.4 Atomic force lithography - "nano-shaving"

The sharp AFM/STM tips can be used not only for studying the topographic or electronic properties, but for modifying the material as well (AFM/STM lithography). There are several types of AFM/STM lithographies: positioning of particles (or even single atoms), manipulating with molecules, indentation, electric modification (local electrostatic charging, anodic oxidation), and others.

The mechanical properties of thin films can be studied by scanning in the contact mode while increasing the scanning force (load). When the threshold force is reached, the tip starts to penetrate into the layer. If the film is thin enough, the penetration can continue down to the substrate and the layer material can be removed - so called nano-shaving [17]. By the nature of penetration and the values of the penetration and removal forces, the structure of the layer and the type of bonding to the surface can be deduced.

2.2 Raman scattering

One type of information is highly difficult to obtain by AFM - chemical composition. Recently, just the first experiments on chemical detection by AFM on atomic scale have been presented [18]. However, they are very challenging and so far applicable only to atomically flat surfaces. Another way how to detect spatially resolved chemical composition is Raman scattering.

It is based on the fact that the interaction of materials with electromagnetic waves can reveal properties of the material. Such interactions are called scattering, as after the interaction the light changes either its direction or wavelength or both. Basically, there are two types of scattering: elastic and inelastic, according to the energy exchange between the light and the material. Rayleigh scattering is an example of elastic scattering (no energy exchange). As its probability is high, it usually dom-

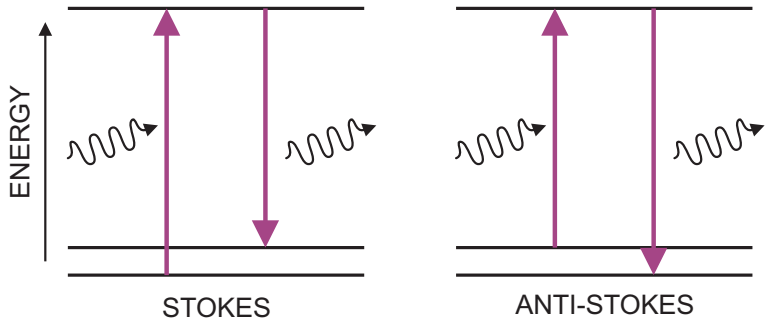

Figure 2.5: *Energetic schemes of the Raman scattering process.*

inates the scattered light. Raman scattering belongs to the inelastic group and is much weaker as its probability is at least seven orders of magnitude lower.

During the Raman process the light changes its energy. The differential energy is given to or obtained from the interacting material as indicated in Fig. 2.5. The process involves energy states between the ground and excited levels. In the Stokes process the light excites an electron from the ground state to the excited state. De-excitation then finishes in a different state than the ground one and the differential energy is given to the material. In other words, the scattered light carries lower energy than the incident one. The so-called anti-Stokes process is inverted - the energy is supplied by the material and the scattered light energy is higher.

Positions of the energy levels are specific for a given material. Therefore, Raman scattering maximum positions are characteristic for each individual material.

The usage of a laser beam as a probe also brings noticeable advantage as an optical beam can be focused down to micrometer diameters. Therefore, the chemical composition can be studied with this resolution. This is the basic idea of micro-Raman mapping. The Raman spectra are collected at a matrix of microscopic points and the peak intensity characteristic for a wanted material is plotted. The resulting map shows a relative concentration distribution of the material. Moreover, the lateral distribution can be complemented by information on the distribution in the z-direction on some materials due to the dependence of absorption depth on wavelength [19].

Chapter 3

ORGANIC BULK-HETEROJUNCTIONS

In this chapter we applied various scanning probe microscopy (SPM) techniques to organic heterostructures. We have shown that already microscopic morphology imaging can detect ordering or local disorder in the blend films. A deeper insight into the bulk-heterojunction blend films is obtained by applying the advanced regimes of SPM. In the articles below we correlate atomic force microscopy (morphology), Kelvin force microscopy (surface potential), current-sensing AFM (local conductivity) with the mapping of micro-Raman spectroscopy. Furthermore, we demonstrate that dynamic optoelectronic processes can be studied locally by advanced SPM regimes as well.

3.1 Preparation of polymer blend thin films

Polymer blend films can be prepared by various techniques (thermal evaporation, spin coating, dip coating, "doctor blade", etc.). In our case, we applied the spin coating technique to achieve reproducible layer homogeneity and thickness. The sample is mounted to a chuck, a solution of the materials in an organic solvent is poured on it and the chuck with the sample starts rotating at desired speed for a certain time period. In the first stages of the process the solution spreads over the substrate surface, the majority is thrown away leaving a thin layer on the surface. Then the rotation helps to dry out the solvent. The drying process is usually finished in an oven or on a hotplate. The quality and structure of the deposited films depends on many factors (e.g. type of solvent, speed and initial acceleration, density and viscosity of the solution, surrounding relative humidity, temperature, ...) and the concrete process parameters are the results of several test depositions.

3.2 Multi-mode microscopic characterization

In the article "Correlation of atomic force microscopy detecting local conductivity and micro-Raman spectroscopy on polymer-fullerene composite films" *(Čermák et al., Phys. Stat. Sol. rrl (2007) **1**, 193-195)* we describe a wide-range study of a blend thin film made of polyfluorene-based polymer and fullerene C_{60}. Such blend film was expected to work as a bulk-heterojunction photovoltaic cell. Highly effective photoluminescence quenching indicated the dissociation of the photogenerated exciton. However, the photovoltaic power conversion efficiency was extremely low (below 0.01 %).

The probable reason for the poor photovoltaic performance of the blend was found when the tapping mode AFM morphology, surface potential (KFM) and conductivity (CS-AFM) measurements were correlated with the microscopic chemical composition information (micro-Raman scattering mapping). The correlation of these four scanning microscopic techniques revealed local microscopic areas lacking one of the two materials. Therefore, we concluded that such areas are not of heterostructural nature any more and that the device is electrically shunted by the conductive polymer. This has been proven as crucial information for further improving the blend technology.

phys. stat. sol. (RRL) **1**, No. 5, 193–195 (2007) / **DOI** 10.1002/pssr.200701131

pss +++rapid research letters+++
www.pss-rapid.com

Correlation of atomic force microscopy detecting local conductivity and micro-Raman spectroscopy on polymer–fullerene composite films

Jan Čermák[*,1], Bohuslav Rezek[1], Věra Cimrová[2], Drahomír Výprachtický[2], Martin Ledinský[1], Tomáš Mates[1], Antonín Fejfar[1], and Jan Kočka[1]

[1] Institute of Physics, Academy of Sciences of the Czech Republic, v.v.i., Cukrovarnická 10, 16253 Prague 6, Czech Republic
[2] Institute of Macromolecular Chemistry, Academy of Sciences of the Czech Republic, v.v.i., Heyrovského náměstí 2, 16206 Prague 6, Czech Republic

Received 13 July 2007, revised 10 August 2007, accepted 13 August 2007
Published online 17 August 2007

PACS 68.37.Ps, 68.55.Nq, 73.50.Pz, 78.30.Na, 81.05.Qk, 81.05.Tp

[*] Corresponding author: e-mail cermakj@fzu.cz

Thin hetero-junction composite films of polymer (electron donor) and fullerene (electron acceptor) are prepared on indium-tin-oxide coated glass by spin-coating from solution in dichlorobenzene. Optimized atomic force microscopy (AFM) parameters allowed us to scan these soft composite films in contact mode and to measure their local conductivity with high lateral resolution by current-sensing AFM. The morphology and local conductivity data are correlated with Kelvin force microscopy and micro-Raman mapping and discussed with view to their photovoltaic properties. Regions with both compounds present are compared to areas where the components segregated, acting as shunts of the junction.

1 Introduction Organic photovoltaic devices [1, 2] are still not able to compete with conventional inorganic solar cells mainly due to the lower power conversion efficiency (~5% [3]). Improvements can be achieved by better understanding the generation and transport of photogenerated charge carriers. In the past the current-sensing atomic force microscopy (CS-AFM) [4, 5] has been used for the study of microscopic morphology and local electronic transport properties of heterostructural silicon thin films, leading to remarkable results [6, 7]. In the CS-AFM, a DC voltage between the sample and the AFM tip is applied when scanning in contact regime and the electric current is detected. Therefore, both microscopic morphology and local conductivity can be characterized simultaneously. Applying this technique to heterostructural organic thin films faces the problem of establishing mechanical and electrical contact to the soft organic materials without compromising their integrity. So far, CS-AFM has been used for a few types of organic materials. Ni-implanted polyethylene terephthalate films needed to be cooled to low temperatures (down to 160 K) for obtaining reliable and reproducible contact-AFM measurements [8]. The study of electrodeposited polypyrrole films by CS-AFM revealed a significant dependence of film conductivity on electrolyte composition [9]. Alexeev et al. studied the electronic and structural properties of a blend of two semiconducting polymers (donor–acceptor system) by CS-AFM [10] allowing only indirect deduction of microscopic material composition and hence relevant electronic properties.

In this work, we report on a successful use of CS-AFM at ambient conditions to obtain reproducible microscopic maps of local conductivity on soft heterostructural organic thin films without any damage. Furthermore, we correlate this data with microscopic morphology measured by tapping mode AFM (TM-AFM), local electron work functions deduced from Kelvin force microscopy (KFM) and material composition detected by micro-Raman spectroscopy. We show that combination of all these techniques enables significantly enhanced insight into the properties of heterostructural composite films.

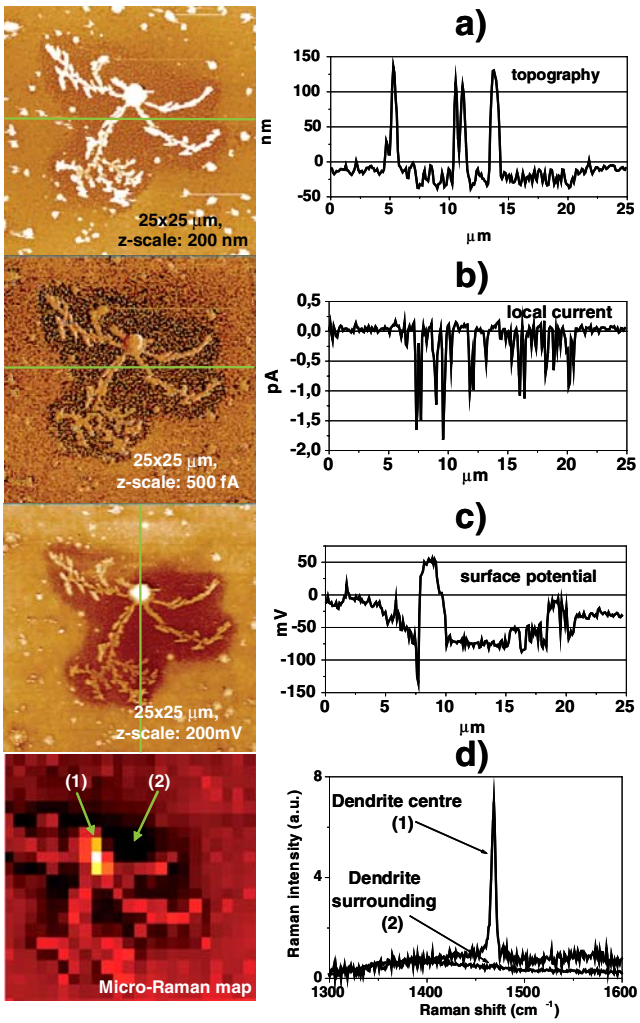

Figure 1 (online colour at: www.pss-rapid.com) Left: a) Tapping mode AFM morphology of organic heterostructure; b) map of local conductivity measured by CS-AFM; c) image of surface potential detected by KFM; d) map of micro-Raman intensity at 1458 cm^{-1} showing relative amount of C_{60}. Green lines in (a)–(c) show the position of the line profiles shown in the graphs to the right. Bottom right graph shows two Raman spectra taken at the positions marked by numbers in the Raman map (d).

2 Experimental Composite thin films were spin-coated from a solution of fullerene C_{60} (Sigma Aldrich) and poly[(2,7-(9,9-dihexa)fluorene)-co-(1,4-(2,5-didecyl-aminoketo)phenylene)] (VYP-120, developed at Institute of Macromolecular Chemistry, ASCR) (weight ratio 4:1 [11]) in 1,2-o-dichlorobenzene on ITO covered glass substrates and dried at 50 °C under vacuum for 4 hours. The resulting film thickness was 50 nm. For characterizing the photovoltaic performance of the films, top Al electrodes were evaporated through a shadow mask.

Film thickness (P-10 profiler by Tencor), photoluminescence (home-made fluorimeter with Xe lamp and photomultiplier detector) and photoelectrical transport (Keithley 237 S-M unit) were measured for macroscopic characterization.

An atomic force microscope (Veeco Dimension 3100) was used to characterize microscopic morphologic and electronic properties. Appropriate cantilevers were used for different scan modes: mid-frequency (75 kHz) cantilevers with reflective Al coating for morphology (tapping mode AFM, TM-AFM) and KFM and low frequency (13 kHz) cantilevers with conductive CrPt coating for CS-AFM. To prevent the AFM tip from damaging the layer the scanning parameters were optimized (contact force: 6 nN, scan speed: 3.75 µm/s, sample bias: –10 V).

A Renishaw inVia Reflex Raman microscope (excitation at 785 nm) was used to characterize the local material composition. The Raman spectra were collected in a matrix of spots and the Raman intensity at 1458 cm^{-1} (C_{60} Raman strongest maximum [12]) was evaluated to obtain a map of lateral distribution of the fullerene. Considering the focal length of the excitation laser beam (1 µm) and the absorption depth of the material at 785 nm (0.8 µm), the Raman spectra were collected from the whole layer volume (layer thickness ~50 nm).

3 Results and discussion In spite of observed quenching of photoluminescence compared to polymer layers without the C_{60}, the composite layers exhibited low photovoltaic power conversion efficiency (I_{sc} ~2 nA; V_{oc} ~5 mV; η ~0.06%).

Morphology (Fig. 1a) scanned by tapping mode AFM (TM-AFM) revealed a relatively flat and smooth surface (RMS roughness: 4 nm) which was covered with two types of clusters (lateral size either ~100 nm or several µm) and dendrites (more than 10 µm). According to the optical microscope image, both the clusters (plenty in an area of 1 mm^2) and dendrites (several per 1 mm^2) are typical objects in the layer.

The local current (Fig. 1b) measured by the CS-AFM at the same field of view was clearly correlated with the morphologic features. The current detected on the dendrite as well as on the clusters varied in the range of 0.1 pA (background noise of the detector was 0.01 pA). In the vicinity of the dendrite and on the edges of the larger clusters the current was an order of magnitude higher (1–1.5 pA; due to the negative sign of the bias applied to the sample, the detected current is negative as well. Therefore, more conductive regions appear darker in Fig. 1b).

The surface potential studied by KFM (Fig. 1c) at the central part of the dendrite was higher than the potential at the small clusters (difference ~80 mV) and large clusters (difference ~20 mV). Higher surface potential (brighter parts in Fig. 1c) stands for lower work function of the material [13].

The micro-Raman mapping in Fig. 1d reveals higher concentration of C_{60} at the dendrite and no C_{60} Raman signal in its close surroundings. Outside of the dendrite area the C_{60} signal is more or less homogeneous.

Homogeneous Raman map outside of the dendrite area indicates that both components of the composite are present and relatively evenly distributed laterally. Yet note

that from the present Raman and AFM data we cannot deduce how well the components are intermixed on a submicrometer scale or what their in-depth distribution is.

The micro-Raman map across the dendrite suggests that the dendrite consists of C_{60} segregated from the nearest surroundings, where only conductive polymer VYP-120 remains. This deduction is corroborated by CS-AFM which detects a one order of magnitude higher conductivity in the dendrite surroundings than in the rest of the sample.

Correlation of the KFM data with micro-Raman map shows that the electron work function of C_{60} is lower than that of the VYP-120 polymer. Such configuration is fundamental for the proper solar cell function with C_{60} as electron acceptor and VYP-120 as electron donor, when behaviour analogous to standard pn-junction solar cell (C_{60} plays the role of n-type semiconductor) is supposed.

However, all the above results also indicate that the area in the vicinity of the dendrite practically lacks the properties of heterojunction and most likely causes shunting of the whole solar cell.

4 Conclusions By optimizing scanning parameters a successful contact-mode CS-AFM measurement of the local electronic transport properties of heterostructural organic thin films has been achieved and correlated with surface potential and micro-Raman mapping. This unique combination of microscopic techniques seems to be a promising tool for the characterization of heterostructured organic thin films as it enables better understanding of their performance in optoelectronic, and in particular photovoltaic, applications.

Acknowledgements This research was supported by AV0Z 10100521, LC510, LC06040, SN/3/172/05, GAAV IAA1010316, IAA1010413, GACR 202/05/H003 and KJB100100512 projects.

References

[1] S. Nešpůrek and J. Pospíšil, J. Optoelectron. Adv. Mater. **7**, 1157 (2005).
[2] Ch. Waldauf, M. C. Scharber, P. Schilinky, J. A. Hauch, and Ch. J. Brabec, J. Appl. Phys. **99**, 104503 (2006).
[3] W. Ma, C. Yang, X. Gong, K. Lee, and A. J. Heeger, Adv. Funct. Mater. **15**, 1617 (2005).
[4] F. Houzé, R. Meyer, O. Schneegans, and L. Boyer, Appl. Phys. Lett. **69**, 1975 (1996).
[5] M. A. Lantz, S. J. O'Shea, and M. E. Welland, Phys. Rev. B **56**, 15345 (1997).
[6] B. Rezek, J. Stuchlík, A. Fejfar, and J. Kočka, J. Appl. Phys. **92**, 587 (2002).
[7] B. Rezek, J. Stuchlík, A. Fejfar, and J. Kočka, Appl. Phys. Lett. **74**, 1475 (1999).
[8] J. Y. Sze, B. K. Tay, C. I. Pakes, D. N. Jamieson, and S. Prawer, J. Appl. Phys. **98**, 066101 (2005).
[9] D.-H. Han, H. J. Lee, and S.-M. Park, Electrochim. Acta **50**, 3085 (2005).
[10] A. Alexeev, J. Loos, and M. M. Koetse, Ultramicroscopy **106**, 191 (2006).
[11] V. D. Mihailethi, L. J. A. Koster, P. W. M. Blom, Ch. Melzer, B. de Boer, J. K. J. van Duren, and R. A. J. Janssen, Adv. Funct. Mater. **15**, 795 (2005).
[12] K. L. Lo and M. C. Lee, Chin. J. Phys. **31**, 653 (1993).
[13] B. Rezek and C. E. Nebel, Diam. Relat. Mater. **14**, 466 (2005).

3.3 Illumination effects and their kinetics

In the article "Optoelectronic performance of poly(*p*-phenylenevinylene)-based heterostructures evaluated by scanning probe techniques" *(Čermák et al., Phys. Stat. Sol. b (2009)* ***246****, 2828-2831)* similar microscopic techniques to those described in the previous section are applied to two organic heterostructures with non-fullerene electron acceptor. Non-fullerene electron acceptor materials are promising due to easier adjustment of optoelectronic properties. We discuss the micro-Raman maps in more detail to detect the contribution of layer thickness to the measured Raman spectra intensity, which may influence the spectra evaluation. We extended the KFM technique to study dynamic electronic processes under illumination as well. Different dynamics and intensity of surface potential shifts under white light illumination indicated different efficiency of charge carrier photogeneration. We also supported this result by current-voltage characteristics measured locally by the AFM tip. Such results corroborate different photogeneration efficiencies measured macroscopically by the photoinduced surface potential decay technique. Thus dynamic KFM was shown to be a reliable microscopic technique for the characterization of dynamic optoelectronic properties of organic heterostructures.

Phys. Status Solidi B **246**, No. 11–12, 2828–2831 (2009) / **DOI** 10.1002/pssb.200982255

physica status solidi b
www.pss-b.com
basic solid state physics

Optoelectronic performance of poly(*p*-phenylenevinylene)-based heterostructures evaluated by scanning probe techniques

Jan Čermák*[,1], Bohuslav Rezek[1], Věra Cimrová[2], Drahomír Výprachtický[2], Hans-Heinrich Hörhold[3], Martin Ledinský[1], and Antonín Fejfar[1]

[1] Institute of Physics, ASCR, v.v.i., Cukrovarnická 10, 162 00, Prague, Czech Republic
[2] Institute of Macromolecular Chemistry, ASCR, v.v.i., Heyrovského náměstí 2, 162 06, Prague, Czech Republic
[3] Institut für Organische Chemie und Makromolekulare Chemie, Universität Jena, Humboldtstraße 10, 07743 Jena, Germany

Received 23 April 2009, revised 5 August 2009, accepted 17 August 2009
Published online 12 October 2009

PACS 64.75.Va, 68.55.am, 73.61.Ph, 78.30.Jw, 78.66.Qn, 85.60.Bt

* Corresponding author: e-mail cermakj@fzu.cz, Phone: +420-220-318-519, Fax: +420-233-343-184

Thin polymer blend films made of donor and acceptor poly(*p*-phenylenevinylene) (PPV)-based polymers were prepared. Diverse scanning probe techniques (atomic force microscopy (AFM), Kelvin force microscopy (KFM), current-sensing AFM (CS-AFM), and micro-Raman mapping) are used to characterize morphologic, electronic as well as optoelectronic properties of the heterostructures. Morphologies of the heterostructures are correlated with microscopic and macroscopic electronic response to a broad-band visible illumination. The data are discussed with respect to photovoltaic applications.

1 Introduction Conjugated polymers are of a high interest for optoelectronic applications due to their relatively easy and inexpensive fabrication and tunable optoelectronic properties [1, 2]. In particular, they are considered promising for photovoltaics. Yet power conversion efficiencies achieved on so-called bulk-heterojunction photovoltaic cells are still too low (5–6% [3, 4]) to compete with inorganic cells. It is assumed that this is caused by imperfections in microstructural ordering of the heterostructures. This view has been recently supported by a correlation of advanced SPM measurements (KFM and CS-AFM) with mapping of chemical composition by micro-Raman spectroscopy on a typical bulk-heterojunction structure [5].

In this paper we report on a systematic study of microscopic morphologic, electronic, and optoelectronic properties of two polymer blends in thin films. We prepared heterostructural blends with both electron donor and acceptor based on PPV. Although the performance of such structures does not reach as high values of photovoltaic conversion efficiency as the blends with a commonly used fullerene-based electron acceptors, they are promising for bulk-heterojunction photovoltaic cells as their properties (absorbance in the visible spectra, probability of aggregation, etc.) can be controlled easier than in the case of fullerene derivatives [6, 7]. In addition to commonly applied scanning probe techniques the illumination-induced effects and their kinetics under a broad-band visible light illumination were studied via changes of surface potential and microscopically detected current–voltage characteristics.

2 Experimental Two types of polymer blends were prepared using TPD-MEH-M3EH-PPV, M3EH-PPV as electron donors, and CN-ether-PPV as electron acceptor (Fig. 1). The average molecular weights and degree of polymerization of the polymers were: M3EH-PPV: $M_n = 8800$, $M_w = 30\,000$, $P_n = 71$; TPD-MEH-M3EH-PPV: $M_n = 29\,100$, $M_w = 74\,900$, $P_n = 61$; and CN-ether-PPV $M_n = 12\,000$, $M_w = 20\,600$, $P_n = 34$. The blends were prepared in the weight ratio 1:1. Synthesis of the materials is described in the literature [8, 9]. Thin films of polymer blends were prepared in the thickness of 100–150 nm by spin-coating (2000 rpm, 60 s) from toluene (TPD-MEH-M3EH-PPV + CN-ether-PPV) and dichlorobenzene (M3EH-PPV + CN-ether-PPV) solutions on Au coated glass substrates (1×1 cm^2). The thin films were annealed at 60 °C for 4 h in vacuum. Preparation process was performed in nitrogen atmosphere.

Microscopic morphologic properties of the films were characterized by the Dimension 3100 (Veeco) atomic force

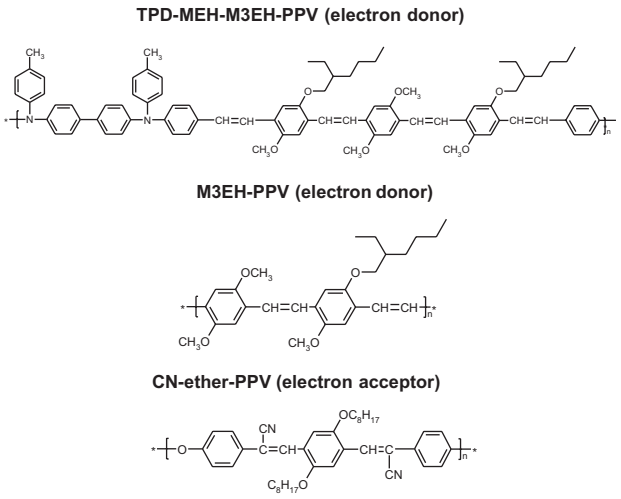

Figure 1 Chemical structures of polymers used for heterojunction preparation.

microscope (AFM) with silicon cantilevers for scanning in tapping-mode (resonance frequency 300 kHz). Pt+Cr coated cantilevers (resonance frequency 75 kHz) were used for Kelvin force microscopy to study illumination induced effects under repeated switching on and off a broad-band visible light source [10] (illuminance at the sample position in the AFM microscope was 500–800 lx). Slow scan axis was disabled during these measurements, i.e. AFM is repeatedly scanning the same line and the *y*-axis represents the time axis.

CS-AFM measurements were performed by the same AFM system with low frequency (13 kHz) Pt+Cr coated cantilevers scanning in contact mode. Typical contact forces were below 10 nN. CS-AFM regime was also used for local current–voltage (*I–V*) measurements by the AFM cantilever. Bias voltage was applied to the sample (Au electrode under the organic layer). Current was detected by the Extended TUNA module (Veeco).

Lateral distribution of chemical composition was studied by the inVia Reflex Raman microscope (Renishaw) using the excitation wavelength of 785 nm. As conjugated polymers absorb mainly in the UV–VIS region, the detected Raman scattering signal is supposed to be generated in the whole layer thickness. The Raman spectra were collected in a matrix of spots with a resolution given by the laser beam diameter (1 μm using 100x objective). Intensity at 1584 cm^{-1} (characteristic Raman scattering maximum of CN-ether-PPV - measured on neat polymer thin film) was used to create a map of relative concentration of the electron acceptor material.

3 Results Figure 2 shows AFM morphology of the polymer blend heterostructures. TPD-MEH-M3EH-PPV + CN-ether-PPV (Fig. 2a) heterostructure exhibits RMS roughness 3.4 nm with autocorrelation length of 2.3 μm. RMS roughness of M3EH-PPV + CN-ether-PPV system

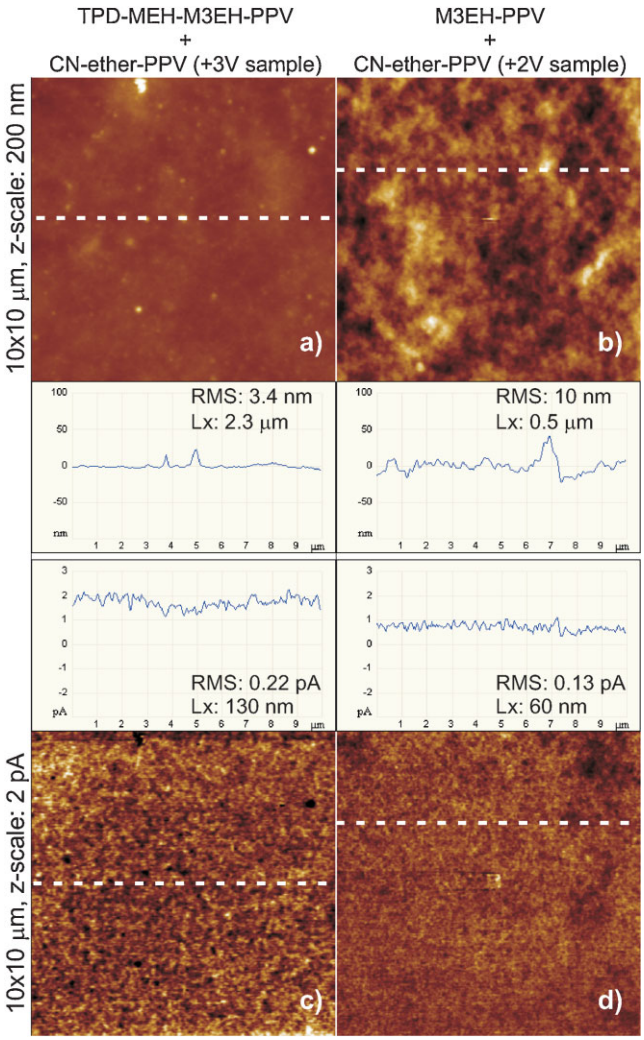

Figure 2 (online color at: www.pss-b.com) a,b) AFM morphology of the heterostrucutres; c,d) maps of local conductivity at the same areas (applied bias voltages: +3 V (c), +2 V (d)).

(Fig. 2b) is higher (10 nm) and its autocorrelation length is shorter (0.5 μm).

Local conductivity maps (Fig. 2c,d) measured by CS-AFM have similar character for both heterostructures. These maps show fluctuations of local currents (RMS 0.13 and 0.22 pA) with autocorrelation lengths 60 and 130 nm. The absolute values of the local currents vary with the applied bias voltage (2 and 3 V) and particular material composition.

KFM measurement on the TPD-MEH-M3EH-PPV + CN-ether-PPV heterostructure (Fig. 3a) shows shift of surface potential by 50 mV under a broad band visible light illumination. This change is fast (within a few seconds) when switching on the illumination. Relaxation to original surface potential takes 3–4 min after switching off the illumination.

KFM on the M3EH-PPV + CN-ether-PPV heterostructure (Fig. 3b) shows smaller shift of surface potential (20–30 mV) under the illumination. The response is also slower

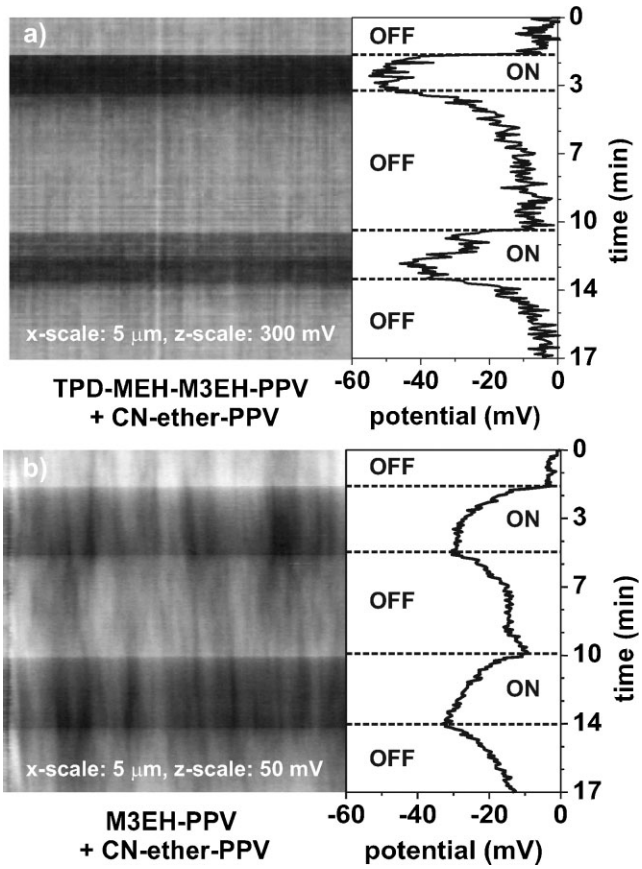

Figure 3 Surface potential variations during illumination switching on and off.

and it is not stabilized after 3 min after switching on the illumination. Relaxation to original value also takes longer. The original surface potential is not reached even after 6 min after switching off the illumination.

Figure 4a shows current–voltage characteristics of TPD-MEH-M3EH-PPV + CN-ether-PPV heterostructure in dark and under the illumination measured by the AFM tip. Both curves exhibit diode-like dependencies with no conductivity in reverse direction and exponential increase in forward direction. Under illumination the slope in forward direction is changed and the current detected at 2 V is almost doubled (4 pA) compared to measurement in dark (2.2 pA).

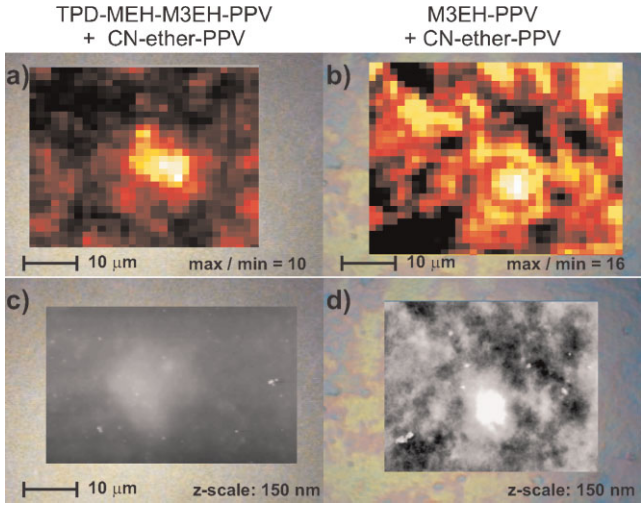

Figure 5 (online color at: www.pss-b.com) Micro-Raman maps of CN-ether-PPV concentration (a,b) and AFM topography at the same areas (c,d).

Figure 4b shows current–voltage characteristic of M3EH-PPV + CN-ether-PPV heterostructure in dark and under the illumination measured by the AFM tip. Hardly any change (within error bar) is detected under illumination.

The micro-Raman map of TPD-MEH-M3EH-PPV + CN-ether-PPV (Fig. 5a) shows typical local region with higher Raman scattering signal of CN-ether-PPV. AFM morphology image (Fig. 5c) shows increased height up to 40 nm at the same area.

The micro-Raman map of M3EH-PPV + CN-ether-PPV (Fig. 5b) shows localized regions of higher CN-ether-PPV Raman scattering intensity. These areas are correlated with the morphological features, according to AFM topography image (Fig. 5d). AFM topography shows height variations in 150 nm range.

4 Discussion The micro-Raman mapping apparently indicates that in both heterostructures the materials are not homogeneously spread. In the Fig. 5a the region with higher concentration of CN-ether-PPV is morphologically raised above the rest of the image. Such increase in height can

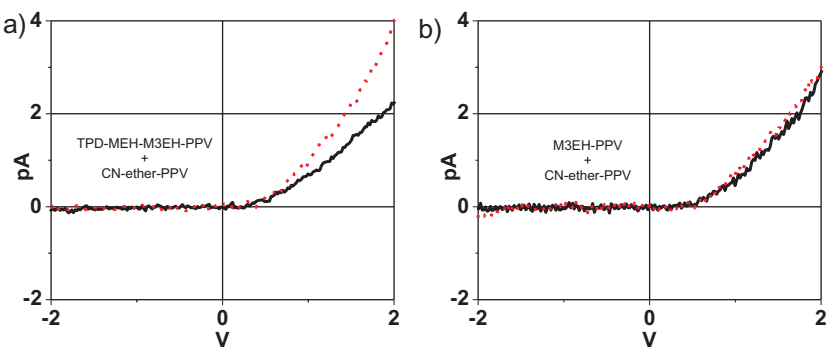

Figure 4 (online color at: www.pss-b.com) Local *I–V* characteristic measured by AFM tip (bias voltage applied to samples) in dark (solid lines) and under a broad-band light illumination (dotted lines).

influence Raman scattering intensity, as the layer is thicker there. However, this increase in height is not that high to induce ten times more intensive Raman signal (maximal/minimal Raman scattering intensity = 10). Therefore, the bright region in the Raman map in Fig. 5a really represents higher concentration of the electron accepting material.

In the M3EH-PPV + CN-ether-PPV system the height variations are comparable to the layer thickness. Therefore, no information about local chemical composition can be deduced, as the Fig. 5b is most likely dominated by the variations of the layer thickness.

In spite of the variations of chemical composition or morphology, microscopic electronic properties look homogeneous. This indicates, that the "sandwich" resistivity is homogeneous, independent of the height variations. This is in agreement with the assumption, that the resistivity should be governed by the heterostructural nature of the mixed layer and not by ohmic resistivity of neat polymers [5]. As electric current flows through the whole layer, it indicates homogeneous electric properties in the bulk volume as well.

The heterostructures under study exhibit high values of photogeneration efficiency, as was measured by the photoinduced surface potential decay technique [11, 12]. Higher values were achieved for the TPD-MEH-M3EH-PPV + CN-ether-PPV blend. Also our measurements of microscopic surface potentials proved that the heterostructures are photosensitive. Shifts of the surface potential (Fig. 3) are attributed to generation and/or redistribution of free charge carriers [10, 13–15]. Similar KFM studies on polypyrrole-diamond heterojunction showed very fast (<1 s) charge carrier generation and recombination. A reference system of polypyrrole-gold interface showed no response, i.e. excitons were not dissociated [10]. Fast shift of surface potential after illumination of the TPD-MEH-M3EH-PPV + CN-ether-PPV heterostructure is therefore most likely caused by fast exciton generation and dissociation. After switching the illumination off, equilibration to original state takes longer due to the spatial separation of free charge carriers. Response to illumination of the other heterostructure is slower, which indicates less effective exciton dissociation.

The *I–V* characteristics exhibit diode-like behavior in agreement with a photovoltaic cell theory. Under illumination a change in the slope of *I–V* characteristic was observed for the TPD-MEH-M3EH-PPV + CN-ether-PPV blend. This corroborates the presence of exciton dissociation to free charge carriers indicated above by surface potential changes. Negligible change of the *I–V* characteristic of the M3EH-PPV + CN-ether-PPV system could be attributed to a lower exciton dissociation efficiency [12] as indicated also by KFM.

Missing shifts of the *I–V* curves under illumination indicate, that in spite of the presence of free charge photogeneration, there is no photocurrent under a short-circuit condition. It may be caused either by insufficient illumination intensity or also by a not optimized bulk-heterojunction inhibits collection of charge carriers to the electrodes. Note, that the shape of the *I–V* characteristic under illumination may be also influenced by the dependence of photogeneration of free charges on electric-field [11, 12].

5 Conclusions Morphologic and optoelectronic properties of thin films of polymer blend heterostructures were studied by various microscopic techniques. It was shown that even when the composition or morphology of the heterostructural blends exhibit large fluctuations their optoelectronic properties can still be homogeneous. Microscopically studied time-resolved photo-response by KFM revealed differences in the efficiency of charge carrier photogeneration. Such results corroborate macroscopic experiments and provide further insight into bulk-heterojunction structure, function, and their mutual correlation.

Acknowledgements We would like to acknowledge the support of MŠMT (grants No. 1M06031, LC06040, and LC510), the GAČR (grant No. 202/09/H041), and GAAV (grants No. KAN400100701, AV0Z10100521, IAA4050409, and the Fellowship J. E. Purkyně).

References

[1] T. Skotheim and J. Reynolds, Conjugated Polymers, Handbook of Conducting Polymers, 3rd ed. (CRC Press, Taylor and Francis Group, 2007).
[2] S. Sun and N. Sariciftci, Organic Photovoltaics (CRC Press, Taylor and Francis Group, 2005).
[3] L. Koster, V. Mihailetchi, and P. Blom, Appl. Phys. Lett. **88**, 093511 (2006).
[4] W. Ma, C. Yang, X. Gong, K. Lee, and A. Heeger, Adv. Funct. Mater. **15**, 1617 (2005).
[5] J. Čermák, B. Rezek, V. Cimrová, D. Výprachtický, M. Ledinský, T. Mates, A. Fejfar, and J. Kočka, Phys. Status Solidi RRL **1**, 193 (2007).
[6] T. Kietzke, Advances in OptoElectronics, DOI: 10.1155/2007/40285 (2007).
[7] M. Mandoc, W. Veurman, J. Sweelssen, M. Koetse, and P. Blom, Appl. Phys. Lett. **91**, 073518 (2007).
[8] H. H. Hörhold, Synth. Metals **119**, 199 (2001).
[9] H. Tilman and H. H. Hörhold, Synth. Met. **101**, 138 (1999).
[10] B. Rezek, J. Čermák, A. Kromka, M. Ledinský, and J. Kočka, Diamond Relat. Mater. **18**, 249–252 (2009).
[11] V. Cimrová, D. Výprachtický, and H. H. Hörhold, Proceedings of the World Polymer Congress – Macro 2006, 41st International Symposium on Macromolecules, CDROM, 2006 (aisystems.com.br), paper 0892.
[12] V. Cimrová, D. Výprachtický, and H. H. Hörhold, Abstract of the 210th Meeting of the Electrochemical Society, p. 408 (2006).
[13] M. Tanimoto and O. Vatel, J. Vac. Sci. Technol. B **14**, 1547 (1996).
[14] S. Saraf, R. Shikler, J. Yang, and Y. Rosenwaks, Appl. Phys. Lett. **80**, 2586 (2002).
[15] A. Liscio, G. D. Luca, F. Nolde, V. Palermo, K. Müllen, and P. Samori, J. Am. Chem. Soc. **130**, 780–781 (2008).

Chapter 4

POLYPYRROLE-DIAMOND SYSTEM

This chapter describes our work on a system consisting of diamond and an organic dye - polypyrrole. From the opto-electronic point of view this system turned out to be similar to the fully organic bulk-heterojunction PV cells described in the previous chapter. The charge carriers are photo-generated in the organic dye (polypyrrole) and, as we found out, they are transferred to the diamond (playing the role of a charge carrier acceptor). The only difference is that in the polypyrrole-diamond case the charge carriers are holes only. This similarity helped us to uncover the photo-generated electronic mechanisms and formulate and prove a model of the charge transfer.

We started with the investigation of the synthesis of polypyrrole on a diamond surface. Then we focused on the redistribution of charge carriers in the system under illumination. Our further experiments were performed to clarify the charge carrier transport and function. Based on the experimental data a model of charge transport from polypyrrole to diamond via interfacial trap states under illumination was proposed. The Hall mobility experiment directly supported the model. The experiments revealed extraordinary optoelectronic properties of the polypyrrole-diamond system compared to metal electrodes and proved that this system is highly promising for the use in opto-electronic as well as bio-electronic applications.

4.1 Diamond as a material

The unique properties of diamond has been well known for a long time. Until just recently, limited resources in nature reduced its application to jewelry. The first attempt to prepare diamond artificially was performed during 1880s by H. Moissan,

but his experiments were hard to reproduce. His technique, now called High Pressure - High Temperature (HPHT), was further improved in the 1940s which started a wider research of diamond as a material. Later on it was shown that diamond can be fabricated by the chemical vapor deposition technique as well. When the chemical vapor deposition is performed on non-diamond substrates, diamond nucleation seeds must be present on the surface to initiate diamond growth. As a result, the CVD diamonds grow as a thin layer consisting of a large number of small monocrystalls - so called nanocrystalline diamond. Its electronic, optical or mechanical properties are not as good as those of monocrystalline diamond, but for many applications they are sufficient.

Generally, diamond is one of the carbon allotropes. It is characterized by the face-centered cubic crystal structure. The atoms are tetrahedrally bonded (sp^3). It is the hardest known material and it is naturally optically transparent. From the electronic point of view it is a wide bandgap ($\sim$ 5.5 eV) semiconductor, which is in its intrinsic form electrically insulating. Diamond can be made electrically conductive by specific doping. The most widely used dopants are boron and phosphorus [20]. Apart from the bulk conductivity induced by doping, intrinsic diamond exhibits a special phenomenon called surface conductivity [21]. It is observed under ambient conditions when the surface atoms of intrinsic diamond are substituted by hydrogen atoms. In this configuration there is a thin (10-20 nm) electrically conductive (p-type) layer formed at the surface. As the surface conductivity phenomenon is conditioned by the termination of the surface by hydrogen atoms, various electrically conductive areas (or paths) can be patterned on the surface [22, 23]. Such patterning is commonly done by termination of the surface by oxygen atoms in a dry oxygen radio frequency plasma discharge using a lithography mask. However, oxygen is not the only substance, that may be attached to the diamond surface whilst influencing the surface electronic properties of diamond [24]. This makes diamond a highly promising component for novel types of devices.

One of the examples are bio-sensors as diamond is chemically stable and well accepted by human body [25]. Their active parts are commonly made of organic materials for their versatility and specific sensitivity. To combine such materials with diamond in applicable devices, first the detailed knowledge about the properties (both mechanical and electronic) at their interface need to be obtained.

4.2 Polypyrrole - a versatile organic dye

For merging with diamond we have chosen polypyrrole for its wide universality as a model of a chemically and optically sensitive organic dye. It is the polymerized form of pyrrole - a heterocyclic aromatic organic material in liquid form consisting of one NH and four CH groups. After polymerization it forms dark and chemically, as well as thermally stable polypyrrole. Such polymerization can be achieved by electrooxidation from a solvent [26], chemical vapor deposition [27], UV irradiation [28] or chemical polymerization [29, 30]. Apart from being a basic structure for other polymeric materials, polypyrrole itself is under intensive study in many fields of applications like sensors [31, 32, 33], biosensors [34, 35], fuel cells [36, 37], corrosion protection [38] or rechargeable batteries [39].

4.3 Electrochemical synthesis of polypyrrole on diamond

The article "Electrochemical synthesis and electronic properties of polypyrrole on intrinsic diamond" *(J. Čermák et al., Diam. Relat. Mater. (2009)* ***18****, 1098-1101)* describes the growth process of polypyrrole on an intrinsic monocrystalline diamond. We synthesized the polypyrrole electrochemically from an aqueous pyrrole solution by the application of a constant current and employing a hydrogen-terminated diamond surface as a working electrode. The force needed for scratching the polypyrrole layer from the diamond surface (measured by AFM) indicated that the two materials are covalently bonded. Our other experiments by Kelvin force microscopy and electric conductivity measurements supported this assumption.

Diamond & Related Materials 18 (2009) 1098–1101

Contents lists available at ScienceDirect

Diamond & Related Materials

journal homepage: www.elsevier.com/locate/diamond

Electrochemical synthesis and electronic properties of polypyrrole on intrinsic diamond

J. Čermák *, B. Rezek, A. Kromka, M. Ledinský, J. Kočka

Institute of Physics, Academy of Sciences of the Czech Republic, v.v.i. Cukrovarnická 10, Prague 6, 162 53, Czech Republic

ARTICLE INFO

Article history:
Received 19 May 2008
Received in revised form 2 December 2008
Accepted 23 January 2009
Available online 31 January 2009

Keywords:
Diamond
Polypyrrole
Electrochemistry
Atomic force microscopy

ABSTRACT

Thin film of polypyrrole is electrochemically deposited on hydrogen terminated surface of intrinsic diamond exhibiting surface conductivity (5×10^{-5} S/□). Based on a high bonding strength (40 nN) estimated by AFM-scratching experiments and local changes of surface work function detected by Kelvin force microscopy we suggest that the polypyrrole is covalently attached to the diamond surface via carbon–carbon bond while replacing the hydrogen termination. Electronic measurements show loss of surface conductivity of diamond after the polypyrrole deposition. These results are discussed in terms of electronic and electrochemical properties of polypyrrole–diamond system also in the perspective of its potential device applications.

1. Introduction

Diamond is not only a well-known gemstone but it is also becoming an interesting industrial material due to its unique properties and the possibility of synthetic growth by chemical vapor deposition [1]. From the electronic point of view, diamond is a wide band gap (5.5 eV) transparent semiconductor. Insulating intrinsic diamond can be changed to p-type or n-type semiconductor by implanting boron or phosphorous. Intrinsic diamond also exhibits 2D surface conductivity when hydrogen terminated (H-diamond) [2]. Preliminary experiments focused on integrated electronic devices based on patterning of the conductive surface have already been reported [3,4].

Diamond also exhibits properties interesting for chemistry and biology. Combination of the biocompatible [5], low chemically reactive [6], optically transparent and mechanically hard diamond [1] with organic and biological materials is expected to lead to wide-range family of novel nanoscaled chemical and biological sensors [7]. These prospects lead to investigations of attachment of organic molecules to diamond. Although diamond is commonly considered chemically inert, its surface can be functionalized. For example, functionalization by alkene, nitrophenyl [6] or DNA [8–11] has been reported recently.

Electrochemistry is one of the techniques that can be used for functionalization of diamond surfaces. This process can be used to cover the conductive electrodes with organic materials from electrolyte. Moreover, when the electrodes are spatially restricted, the deposition area can be precisely localized. We envision that such process might be used for preparation of nanoscaled sensors. Their specific sensitivity could be controlled by the size, nanostructure and other properties of particular organic material.

One class of organic materials, conjugated polymers, has not been studied on diamond so far. Yet they are of potentially high interest as they exhibit electrical conductivity, non-linear optical response and pronounced chemical sensitivity. A typical example is polypyrrole (PPy) [12–14].

Study of the basic principles of the electrochemical deposition and linking process of the organic molecules to diamond surface are of key importance for further device development.

In this paper we report on electrochemical synthesis of PPy thin film from aqueous solution on H-diamond surface. The PPy-diamond system is further characterized by diverse atomic force microscopy (AFM) and electronic transport techniques to determine microscopic morphologic, chemical and electronic properties of the system.

2. Experimental

PPy synthesis was performed on a bulk intrinsic monocrystalline H-terminated diamond (Element 6). The surface of diamond was hydrogen-terminated by microwave plasma (power: 1100 W, temperature: 850 °C, pressure: 30 mbar, H2 gas flow: 300 sccm). Au electrodes were thermally evaporated to provide stable electrical contact. PPy was electrochemically deposited from solution of pyrrole (240 mM; Aldrich) and NaCl (100 mM) in deionised water.

The electrochemical deposition (setup in Fig. 1a) was performed in galvanostatic regime, applying the current −500 nA (Fig. 1b; current density approximately 0.3 mA/cm^2) for 2–3 min by a source-measure unit (Keithley) on the counter electrode (Pt). The diamond as a working electrode was grounded. Subsequent characterizations were

* Corresponding author. Fax: +420 233 343 184.
E-mail address: cermakj@fzu.cz (J. Čermák).

0925-9635/$ – see front matter © 2009 Elsevier B.V. All rights reserved.
doi:10.1016/j.diamond.2009.01.035

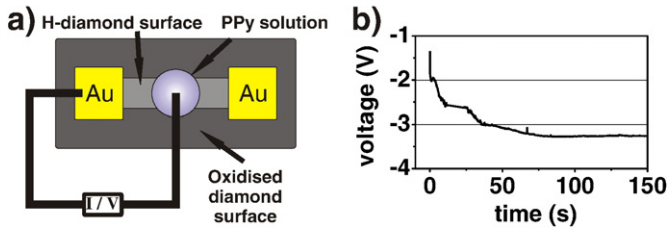

Fig. 1. a) Setup for electrochemical deposition of PPy from aqueous solution on H-diamond surface. b) Typical chronopotentiogram captured during electrochemical deposition of PPy with −500 nA constant current.

done after several (>10) hours under ambient conditions (relative humidity 20–35%) at room temperature to ensure proper drying of PPy.

Dimension 3100 (Veeco) AFM microscope was used for characterization of morphologic and electronic properties and for nanolithographic modification of the PPy film. High frequency (250–300 kHz) Si cantilevers were used for scanning the morphology in tapping mode and for AFM-scratching [8] of the PPy by applying contact forces in the range of 2–5 μN. Mid-frequency (50–100 kHz) Si cantilever with Pt/Ir coating were used for detection of surface potential by Kelvin force microscopy (KFM). The mid-frequency cantilevers without the coating were also used for scanning in contact mode with increasing contact force (19–110 nN) to detect the threshold for penetrating and scratching away the PPy film.

Renishaw inVia Reflex Raman microscope (excitation wavelength 785 nm) was used to detect the formation of PPy on diamond. The micro-Raman spectra were collected in a matrix of microscopic spots. Lateral resolution is given by the diameter of the focused laser beam (1 μm with 100x objective). The Raman intensity at 1600 cm^{-1} (PPy strongest Raman scattering maximum [15]) was used to generate a map of PPy lateral distribution.

Conductivity of the diamond surface was characterized by current–voltage measurements. Instrumental setup was similar to the one used for the electrochemistry with point probe electrodes. One electrode was always connected to Au contact pad on H-diamond. The second electrode was placed directly on the diamond surface to probe particular areas.

3. Results

After the electrochemical deposition, AFM detected a dense and smooth PPy film (RMS roughness ~3 nm at the area of $10\times20\,\mu m^2$) on diamond surface. Thickness of the PPy film was 25 nm based on the height histogram of tapping-mode AFM image (Fig. 2a). This corresponds to rather long PPy chains as 1 pyrrole monomer is 0.75 nm long (result of Density Functional Theory modelling using Euro Fireball software [16,17]). The AFM image taken after scanning the PPy in

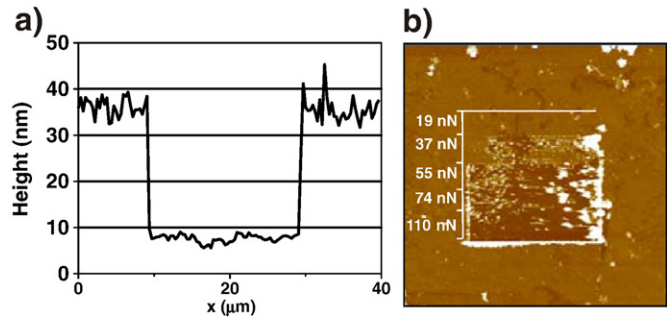

Fig. 2. a) Section of the AFM image after the PPy removal. b) Scratching of the PPy film by AFM tip with increasing contact force. Forces reaching 40 nN are strong enough to affect the PPy film.

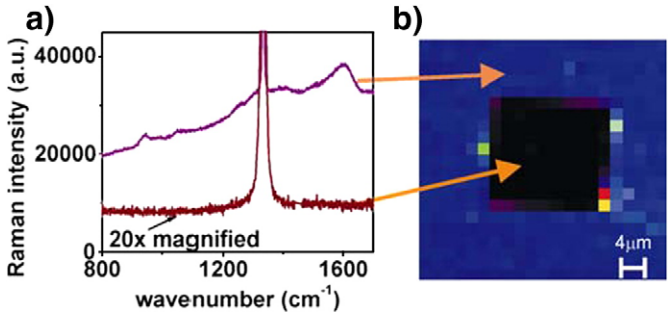

Fig. 3. a) Typical Raman spectra collected from the PPy layer and from the diamond after PPy removal (central square). b) Map of PPy lateral distribution generated by evaluating the intensity at 1600 cm^{-1} (PPy Raman scattering maximum). The intensive maximum at 1332 cm^{-1} is attributed to diamond.

contact mode with increasing contact forces is shown in Fig. 2b. Applying forces above 40 ± 20 nN leads to removal of the PPy film. The error bar was determined from the AFM-scratching experiment, where the contact force 19 nN did not modify the PPy film.

In the micro-Raman map (Fig. 3b) obtained after the AFM-scratching the area of $20\times20\,\mu m$, two types of regions can be distinguished: central square without any detectable signal of PPy and the surrounding PPy layer. Corresponding typical spectra are shown in Fig. 3a. Note that the most intensive Raman scattering maxima of polypyrrole and diamond lie at 1600 cm^{-1} and 1332 cm^{-1} respectively [15,18]. This proves that the PPy was completely removed during the AFM scanning in contact mode using a high contact force (up to 5 μN).

The $I(V)$ measurements (Fig. 4) performed after the PPy growth showed that the conductivity of the diamond surface completely disappeared. Even after polypyrrole removal and exposure to 0.8 M HCl the surface conductivity has not been restored as would be expected based on H-diamond properties [19]. Areas that were not covered by the PPy film remained conductive.

The surface potential differences measured by KFM between the PPy and the diamond after PPy removal was −190 mV and between the PPy and the untreated H-diamond was −80 mV. The configuration of surface potential with respect to the reference Au layer (work function 5.0 ± 0.1 eV as measured by UPS) is shown in Fig. 5. Error bars were determined as the root-mean-square fluctuations of surface

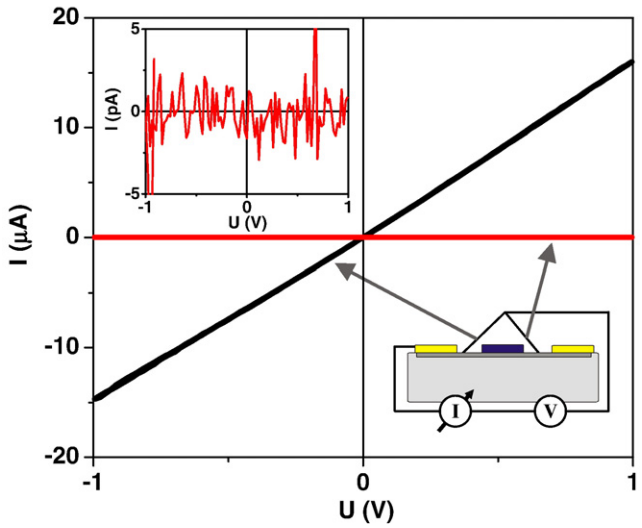

Fig. 4. *I–V* curves measured across original H-diamond (conductive), across diamond with PPy on the surface, and across diamond after PPy mechanical removal (both highly resistive); the insets show the highly resistive characteristics with magnified y-axis and a schematic image of the measurement setup.

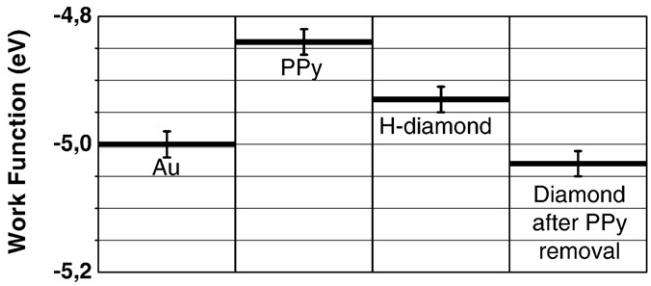

Fig. 5. Scheme of the work functions in the PPy-diamond system as measured by KFM with respect to gold layer (work function -5.0 ± 0.1 eV based on the UPS). Root-mean-square fluctuations of the surface potential during KFM measurements were used to estimate the error bars.

potential. Under illumination by a broad band visible light, the surface potentials of both PPy and the diamond, where PPy was removed, increased by +120 mV and +190 mV. This surface photovoltage effect corresponds to the lowering of surface work function [18].

4. Discussion

Forces needed to remove the PPy film from diamond surface depend on the established bonding type. The bonding strength as measured by the AFM-scratching experiment was estimated to be close to 40 nN. Although the error bar may seem large, such value is still much higher than the value expected for electrostatic or Van der Waals forces (<5 nA [8]) and indicates covalent bonding of PPy to diamond [6,8,20,21].

As for the microstructure of the PPy layer, there are several signs suggesting monolayer structure. Disturbances similar to sweeping snow with a stick were observed when AFM-scratching was applied on DNA layers which were merely adsorbed on diamond [21]. On the other hand, covalently bound DNAs were ripped off the surface in the similar way as the PPy in this work. Multilayer can be recognized also during the AFM-scratching experiment. AFM tip would create several height steps in the layer with increasing contact force [22]. In the case of PPy on diamond, the AFM tip got directly to the diamond surface after reaching the threshold contact force. Therefore the monolayer configuration can be reasonably assumed.

Crucial conditions for generation of surface conductivity on diamond are the H-termination and electron acceptor system (e.g. aqueous electrolyte) on its surface [2,19]. A strongly adsorbed matter may also influence the surface conductivity. But if it is not chemically bound, the surface conductivity should recover after the matter was removed. As the surface conductivity did not recover after exposure to acid, which should promote the surface conductivity, the reason must be the missing H-termination. This conclusion is supported by the KFM measurements as well. Surface potential differences indicate that the work function of the diamond where PPy has been removed is by approximately 120 mV higher than on original H-diamond. Similar effect was also reported for DNA-functionalized diamonds [6]. The complete removal of the PPy was proved by micro-Raman mapping. The negative shift of surface potential difference indicates increase of H-diamond work function. This shift may be attributed to missing H-termination which generates negative electron affinity.

Another indication of missing H-termination is the behaviour of surface potential under illumination. The measured positive change of 190 mV is opposite to what was reported for purely H-terminated diamond [23]. Details of this observation will be reported elsewhere.

Based on these results a model of electrochemical growth of PPy on H-diamond is proposed. During the electrochemistry the H-termination is substituted by the PPy molecules which are covalently attached. Note that complete replacement of all hydrogen atoms by PPy molecules is impossible, as PPy molecules are much larger than hydrogen atoms. Yet, at the present electrochemical deposition conditions, the replacement is efficient enough to destroy the surface conductivity completely and permanently. This is in contrast to previous studies which reported only 5–10% replacement efficiency when using photo- or electrochemical linker molecules and remaining surface conductivity [24].

Yet also other mechanisms of removing the H-termination have to be considered. A variable potential needed to maintain the predefined constant current during the electrochemical deposition can oxidize the diamond surface via anodic oxidation [25,26]. For oxidation, the diamond must be positively biased with respect to the electrolyte. This is also the case during electropolymerization of pyrrole on the diamond surface. However, because diamond exhibits large electrochemical window, starting potential for local anodic oxidation of diamond is typically 4 V [3]. Moreover, the potential drop across the surface conductive layer (resistance of our H-diamond was 20 kΩ) resulted in somewhat lower potential on the diamond surface in the electrochemically active area. Therefore, we conclude that the effect of anodic oxidation of the diamond surface during PPy synthesis is in our case negligible.

5. Conclusions

PPy layer was formed by electro-polymerization on H-terminated intrinsic diamond surface. Characterization of morphologic, electronic, and chemical properties of the resulting PPy-diamond system indicated that the PPy is most likely covalently attached to the diamond surface instead of hydrogen atoms. The substitution of H-termination leads to the complete loss of diamond surface conductivity. We should stress that this is not a detrimental effect. First of all, the hydrogen replacement efficiency may be reduced by decreasing the amount of charge transferred during electrochemical reaction. Second, the high efficiency of PPy bonding and consequent loss of surface conductivity may also become useful for fabricating in-plane organic-diamond devices.

Acknowledgments

We gratefully acknowledge Ing. V. Jurka for lithographical microstructuring of the samples, Dr. A. Fejfar, for software development, and Dr. J. Zemek for UPS measurements. This research was supported by the projects KAN400100701 (GAAV), LC06040 (MŠMT), LC510 (MŠMT), 202/05/H003 (GAČR), AV0Z 10100521, and the Fellowship J.E. Purkyně (GAAV).

References

[1] C.E. Nebel, Nat. Matters 2 (2003) 431.
[2] F. Maier, M. Riedel, B. Mantel, J. Ristein, L. Ley, Phys. Rev. Lett. 85 (2000) 3472.
[3] B. Rezek, J.A. Garrido, C.E. Nebel, M. Stutzmann, E. Snidero, P. Bergonzo, Phys. Status Solidi A 193 (2002) 523.
[4] H. Kawarada, Y. Araki, T. Sakai, T. Ogawa, H. Umezawa, Phys. Status Solidi A 1 (2001) 79.
[5] M. Kalbáčová, M. Kalbáč, L. Dunsch, A. Kromka, M. Vaněček, B. Rezek, U. Hempel, S. Kmoch, Phys. Status Solidi B 11 (2007) 4356.
[6] D. Shin, B. Rezek, N. Tokuda, D. Takeuchi, H. Watanabe, T. Nakamura, T. Yamamoto, C.E. Nebel, Phys. Status Solidi A 203 (2006) 3245.
[7] A. Härtl, E. Schmich, J.A. Garrido, J. Hernando, S.C.R. Catharino, S. Walter, P. Feulner, A. Kromka, D. Steinmüller, M. Stutzmann, Nat. Matters 3 (2004) 736.
[8] B. Rezek, D. Shin, T. Nakamura, C.E. Nebel, J. Am. Chem. Soc. 128 (2006) 3884.
[9] K. Takahashi, M. Tanga, O. Takai, H. Okamura, Diam. Relat. Mater. 12 (2003) 572.
[10] R.J. Hamers, J.E. Butler, T. Lasseter, B.M. Nichols, J.N. Russel Jr., K.-Y. Tse, W. Yang, Diam. Relat. Mater. 14 (2005) 661.
[11] T. Ando, K. Yamamoto, M. Matsuzawa, Y. Takamatsu, S. Kawasaki, F. Okino, H. Touhara, M. Kamo, Y. Sato, Diam. Relat. Mater. 5 (1996) 1021.
[12] B.A. Bolto, D.E. Weiss, Aust. J. Chem. 16 (1963) 1076.
[13] P. Santhosh, N.S. Kumar, M. Renukadevi, A.I. Gopalan, T. Vasudevan, K.-P. Lee, Anal. Sci. 23 (2007) 457.
[14] D.P. Quan, T.W. Lewis, G.G. Wallace, P.H. Viet, Anal. Sci. 17 (2001) i745.
[15] J. Mikat, I. Orgzall, H.D. Hochheimer, Phys. Rev. B 65 (2002) 174202.
[16] J.P. Lewis, K.R. Glaesemann, G.A. Voth, J. Fritsch, A.A. Demkov, J. Ortega, O.F. Sankey, Phys. Rev. B 64 (2001) 195103.

[17] P. Jelinek, H. Wang, J.P. Lewis, O.F. Sankey, J. Ortega, Phys. Rev. B 71 (2005) 235101.
[18] S.A. Solin, A.K. Ramdas, Phys. Rev. B 1 (1970) 1687.
[19] S.G. Ri, T. Mizumasa, Y. Akiba, Y. Hirose, Jpn. J. Appl. Phys. 34 (1995) 5550.
[20] J. Wang, M.A. Firestone, O. Auciello, J.A. Carlisle, Langmuir 20 (2004) 11450.
[21] B. Rezek, D. Shin, C.E. Nebel, Langmuir 23 (2007) 7626.
[22] H. Uetsuka, D. Shin, N. Tokuda, K. Saeki, Ch. Nebel, Langmuir 23 (2007) 3466.
[23] B. Rezek, C.E. Nebel, Diam. Relat. Mater. 14 (2005) 466.
[24] C.E. Nebel, D. Shin, D. Takeuchi, T. Yamamoto, H. Watanabe, T. Nakamura, Diam. Relat. Mater. 15 (2006) 1107.
[25] R.S. Becker, J.A. Golovchenko, B.S. Swartzentruber, Nature 325 (1987) 419.
[26] E.S. Snow, W.H. Juan, S.W. Pang, P.M. Campbell, Appl. Phys. Lett. 66 (1995) 1729.

4.4 Energy bands and surface photovoltage

In the article "Photovoltage effects in polypyrrole-diamond nanosystem" *(B. Rezek et al., Diam. Relat. Mater. (2009)* ***18****, 249-252)* a polypyrrole-diamond system is prepared in a similar way as described in the previous article. We used the AFM tip to remove the polypyrrole from a small area (10×10 μm). This area and its surroundings are studied by Kelvin force microscopy in the dark and under white light illumination. The Kelvin force microscopy data were the source for setting up the energy band scheme of this system. Shifts of the surface potential under illumination observed on the polypyrrole-diamond system and bare diamond are attributed to a sub-surface photovoltage effect which indicates an efficient dissociation of excitons at the polypyrrole-diamond junction and a transfer of holes from polypyrrole to diamond.

Diamond & Related Materials 18 (2009) 249–252

Contents lists available at ScienceDirect

Diamond & Related Materials

journal homepage: www.elsevier.com/locate/diamond

Photovoltage effects in polypyrrole–diamond nanosystem

B. Rezek *, J. Čermák, A. Kromka, M. Ledinský, J. Kočka

Institute of Physics AS CR, Cukrovarnická 10, 162 53 Prague, Czech Republic

ARTICLE INFO

Available online 5 August 2008

PACS:
68.37.Ps
73.40.Lq
73.61.Ph
81.05.Uw

Keywords:
Diamond
Polymers
Heterojunction
Kelvin force microscopy

ABSTRACT

Thin films of polypyrrole (PPy) are electrochemically polymerized in the thickness 25 nm on hydrogen-terminated intrinsic diamond surface exhibiting two-dimensional surface conductivity of 5×10^{-5} (S/). Opto-electronic properties of the system are characterized by Kelvin force microscopy detecting surface potentials. Shifts of the surface potentials of diamond and PPy under visible light illumination are attributed to sub- and super-band gap surface photovoltage effects changing energetic band bending in the range of 100–200 meV. We present a model considering influence of diamond surface termination, surface states and highly resistive bulk properties as well as excitonic transport in PPy. The model suggests a charge transfer between PPy and diamond.

1. Introduction

Combining advantages of optical transparency, hardness [1], low chemical reactivity [2], and biocompatibility [3] of diamond with organic and biological materials is expected to lead to a wide-range of novel nanoscaled chemical and biological sensors [4] and opto-electronic devices [5]. Nowadays, the basic characteristics of such systems are intensively studied to enable further device development.

From the electronic point of view, diamond is a wide band gap inorganic semiconductor (5.5 eV). Intrinsic diamond is thus electrically insulating and transparent for visible light. This feature is employed in development of ultra-violet sensitive photodiodes [6]. The intrinsic diamond can be transferred to p- or n-type semiconductor by boron [1] or phosphorous [7] doping. Also when the intrinsic diamond is hydrogen-terminated (H-diamond), a thin (<10 nm) conductive layer is formed close to the diamond surface under ambient conditions [8]. Moreover, diamond exhibits persistent photoconductivity [9] and interesting excitonic properties [10] as well. Thus merging of diamond with organic dyes may reveal new phenomena and enable novel applications.

Promising class of organic materials for opto-electronics are conjugated polymers. Light emitting diodes or field effect transistors made of organic materials are reaching or even exceeding qualities of inorganic devices today [11]. Polypyrrole is one of the most studied examples. It can be synthesized by electro-polymerization from aqueous solution of pyrrole. When polymerized, conjugated chains of polypyrrole are formed which are electrically conductive and chemically stable [12] with optical absorption in the visible spectral region [13].

In this paper we report on opto-electronic properties of PPy–diamond system of few nanometer thickness. We apply Kelvin force microscopy (KFM) to resolve local surface photovoltage (SPV) effects. We discuss electronic configuration of the heterogeneous system, mechanisms of potential shifts under the illumination, and we deduce a charge transfer between PPy and diamond.

2. Experimental

Synthetic bulk monocrystalline intrinsic (undoped) IIIa CVD diamonds (Element 6) were H-terminated in hydrogen microwave plasma (850 °C, 30 mbar, 1100 W). After exposure to ambient air, the diamonds exhibited surface conductivity of 5×10^{-5} (S/). Au electrodes were thermally evaporated to provide stable electrical contacts. The PPy was deposited from the solution of pyrrole (0.24 M, Aldrich) and NaCl (0.1 M) in deionized water under galvanostatic regime at constant current density of −0.3 mA/cm^2. The electrochemical synthesis was driven by a source-measure unit (Keithley) employing diamond surface as a working electrode. The setup is schematically shown in Fig. 1. Similar synthesis was also performed on a gold film for comparison.

Microscopic morphologic properties of the PPy–diamond system were characterized by atomic force microscope (AFM) with silicon cantilevers scanning in tapping-mode (resonance frequency 300 kHz). The same cantilevers were also used for removing the deposited PPy film from a small area (20×20 μm^2) by scanning in a contact mode using high contact force (2–5 μN), so called nanoshaving [14].

* Corresponding author. Tel.: +420 220 318 525; fax: +420 220 318 468.
E-mail address: rezek@fzu.cz (B. Rezek).

0925-9635/$ – see front matter © 2008 Elsevier B.V. All rights reserved.
doi:10.1016/j.diamond.2008.07.019

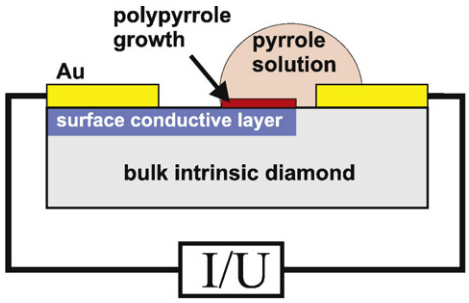

Fig. 1. Schematic setup of PPy–diamond electrochemical synthesis.

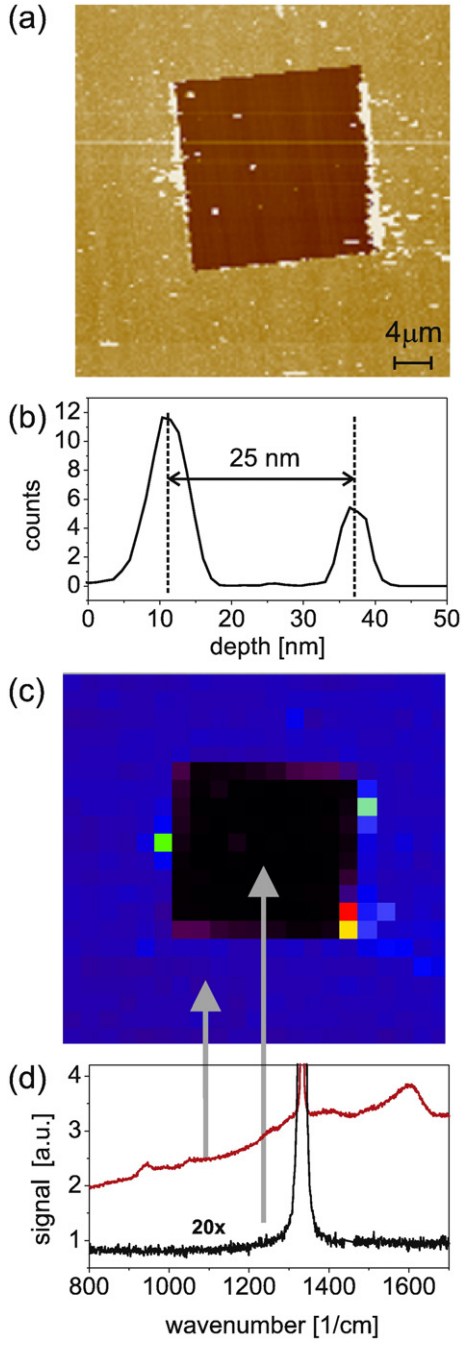

Fig. 2. (a) AFM topography of the area, where PPy was removed by AFM nanoshaving, and its surroundings. (b) Height histogram of AFM topography. (c) Map of Raman scattering intensity at 1600 cm^{-1} at the same area. (d) Typical Raman spectra inside and outside the nanoshaved area.

For the KFM characterization, Pt/Cr coated mid-frequency (75 kHz) cantilevers were used. Metal coating of the tips prevents contribution to SPV from silicon. Dark conditions during measurements were provided by optically non-transparent cover of the AFM. The internal broad-band visible light source of the AFM with controllable intensity was used for measurements under illumination via optical fiber. The maximum illuminance at the sample position in the AFM microscope was 500–800 lx. Influence of the red laser diode (LD) detecting cantilever deflections was neglected because diamond is transparent in visible light and PPy absorbs mostly in blue region (below 500 nm)[13]. Moreover, a major part of the LD beam is screened by the cantilever.

Lateral distribution of chemical composition was detected by the inVia Reflex Raman microscope (Renishaw) using excitation wavelength of 785 nm. The Raman spectra were collected in a matrix of spots with a resolution given by the laser beam diameter (1 μm using 100× objective). The Raman scattering intensity at 1600 cm^{-1} (PPy strongest Raman scattering maximum [15]) was evaluated to generate the map of PPy lateral distribution.

3. Results

After the electrochemical deposition, the surface of diamond is covered by a dense and smooth layer of PPy (root mean square (RMS) roughness about 2 nm at the area of 10×20 μm^2). RMS roughness of the original diamond surface was 0.8 nm at the area of 10×10 μm^2. Fig. 2(a) shows AFM topography of the area where PPy was removed by nanoshaving in the central part. The thickness of the deposited PPy layer was 25 nm (evaluated from the height histogram across the nanoshaved region in Fig. 2(b)), which corresponds to rather long PPy

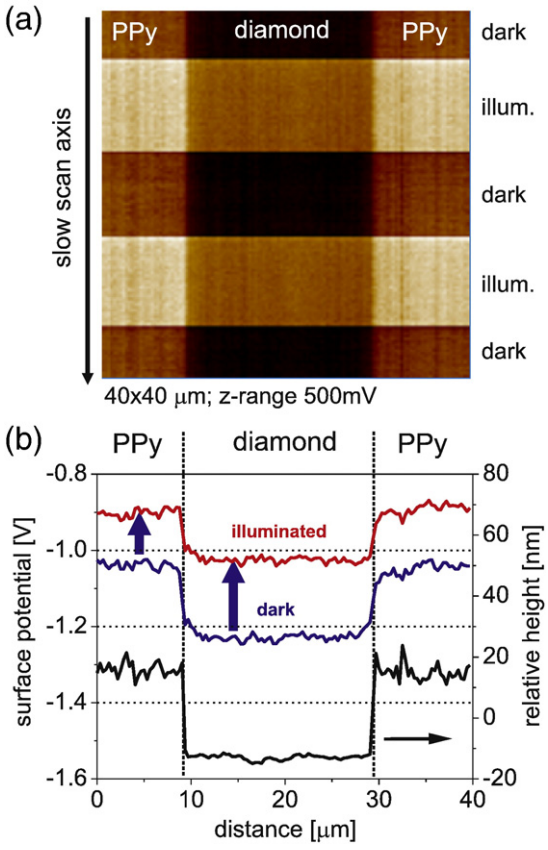

Fig. 3. (a) Map of surface potential measured during illumination on/off-switching on diamond where PPy was removed by nanoshaving (diamond) and on diamond with PPy layer on top (PPy). Surface potential was measured along a single line (slow scan disabled) and only illumination was changing. (b) Typical potential and height line profiles across PPy–diamond–PPy interface.

chains as one pyrrole molecule is 0.75 nm long (based on the Density Functional Theory modelling [16,17]).

The micro-Raman map of polypyrrole characteristic peak at 1600 cm^{-1} in Fig. 2(c) proves that the PPy was completely removed by the AFM nanoshaving. The complete Raman spectra in Fig. 2(d) show characteristic PPy features in the non-shaved region [15] while only diamond peak at 1333 cm^{-1} is detected in the nanoshaved region. Therefore, all further measured opto-electronic properties at the nanoshaved region are attributed to the diamond surface and not to any residual PPy molecules. As PPy attachment is covalent [18], exposed diamond surface is not H-terminated and most likely carbon or oxygen terminations prevail.

This is in agreement with the observation, that after the PPy deposition the diamond surface lost completely the conductivity [18]. Even after the PPy removal and exposure to 0.8 M HCl the conductivity did not recover as would be expected for a H-terminated surface [19]. Areas not covered by the PPy remained conductive.

KFM measurements in Fig. 3 show that under dark conditions there is a surface potential difference of 190 mV between PPy deposited on diamond and the diamond, where PPy was removed by nanoshaving. Under the illumination, increase of surface potentials was observed, namely 120 mV for PPy–diamond and 190 mV for nanoshaved diamond surface. The potential difference between PPy–diamond and nanoshaved diamond is thus effectively reduced by 70 mV (from 190 mV to 120 mV).

Only negligible or no shifts of surface potential on PPy were detected on the control sample, where PPy was electrochemically grown on a gold electrode. Fig. 4 demonstrates shifts of <10 mV upon illumination.

4. Discussion

KFM experiments on PPy–diamond or C-terminated diamond are untypical in a sense that the samples are inherently not grounded because bulk diamond is intrinsic and surface conductivity was removed by PPy synthesis. Yet even on non-conductive samples the KFM is possible [20]. We have also proved on the control sample (PPy–Au) that disconnecting the ground did not have any noticeable effect on the potential contrast.

To understand the KFM results, we have to analyze an electronic configuration of the system. The PPy is a p-type semiconducting material with hole trap states at 0.1–0.4 eV above the HOMO [21]. The density of these trap states is particularly pronounced in thin films with high surface-to-volume ratio. The HOMO is reported to be situated at −5.0 eV with respect to vacuum level [22]. As a result, the trap states are positioned between −4.6 and −4.9 eV below the vacuum level. This is in agreement with the observed potential on PPy in the dark, which is about 0.16 eV higher compared to a gold reference, work function of which was measured by XPS at −5.0 eV [18]. This configuration leads to a downward band bending at PPy surface.

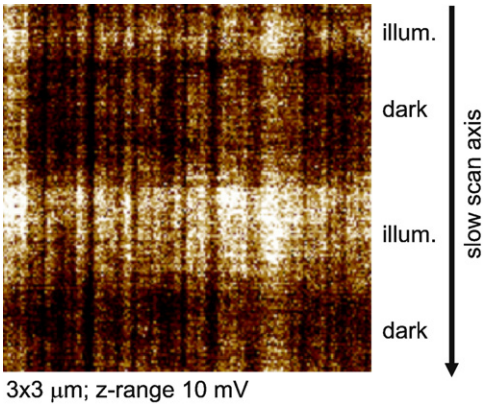

Fig. 4. Map of surface potential measured during illumination on/off-switching on a gold electrode with electro-polymerized PPy film. Surface potential was measured along a single line (slow scan disabled) and only illumination was changing.

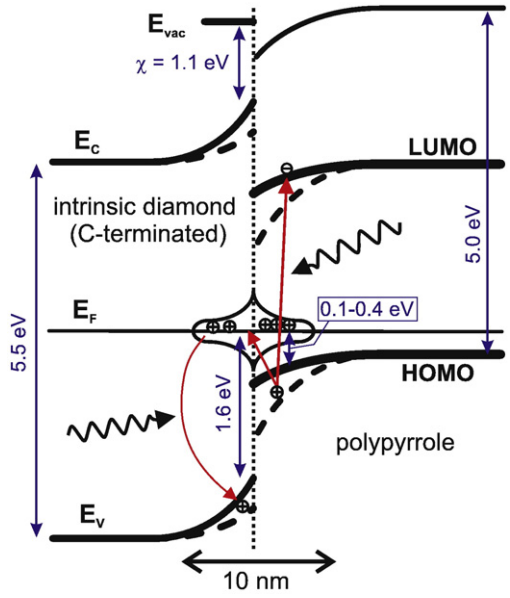

Fig. 5. Energetic scheme of the PPy–diamond system in equilibrium in the dark (full line) and under visible light illumination (dashed line).

The diamond surface, where PPy was removed, can be considered carbon-terminated (C-diamond) as PPy creates covalent bonds. [18] Diamond below PPy can be considered also C-terminated, although average bond saturation is most likely different. By hydrogen removal, surface defect states, which can act as donor-like hole traps, are generated around 1.6 eV above valence band maximum [23,24]. Fermi level of C-diamond lies approximately at 2.3 eV above the valence band maximum in equilibrium [25], which is slightly higher than the trap states. Assuming high positive electron affinity (up to 1.3 eV on reconstructed (100) C-diamond [26]) and typical diamond band gap of 5.5 eV, the trap states are situated around −5.2 eV below the vacuum level. This is in a reasonable agreement with the observed potential on diamond in the dark, which is about 0.03 eV lower than the gold reference work function of −5.0 eV [18]. Looking from the other side, if we take trap energy at 1.6 eV as obtained by de-hydrogenation experiments, which are the closest to our electrochemical process, the diamond electron affinity will be 1.13 eV on our samples. This is within the range of reported values of 0.5–1.3 eV [24].

It should be pointed out that the diamond bulk is highly resistive, hence no bulk carrier diffusion compensating the surface charge can take place. The band bending is thus accomplished rather by dielectric polarization of the diamond sub-surface region. This configuration of energetic bands is confirmed by KFM as discussed further below.

Based on the above description we can assemble the energy band configuration of the PPy–diamond system. The diagram is schematically shown in Fig. 5. The HOMO and surface trap states of PPy are slightly higher in energy than the hole trap states of C-diamond. Therefore, in the PPy–diamond system the holes from diamond will tend to “move” to the PPy trap states. This will increase the occupation of the trap levels and hence also the PPy band bending. One may ask though, where the holes are coming from in the intrinsic diamond. We remind that we start with H-terminated diamond with two-dimensional p-type surface conductivity. To facilitate the electropolymerization of PPy, electrons are transferred from pyrrole to diamond and vice versa holes to PPy. As reaction proceeds, hydrogens

become replaced by bonds to PPy chains and surface states arise in diamond where some of the free holes are trapped and surface conductivity is diminishing. In the end, the diamond is non-conducting (in the dark) and there are holes in both diamond and PPy surface states.

Under illumination, the observed positive shifts of surface potentials correspond in principle to a decrease of work functions [27,20] in both PPy and diamond as indicated in Fig. 5. Comparison of forbidden energy band gaps of PPy (2–3 eV) and diamond (5.5 eV) with a broad-band visible light energy (1.5–4.0 eV) indicates different light-induced mechanisms. Broad-band visible light excitation of diamond is a sub-band gap process in contrast to the PPy, where it is a super-band gap process.

In the case of diamond, trapped holes can be excited to the valence band. Such process has been actually used to characterize the density of trap states by photocurrent spectroscopy [28]. Accumulation of holes in the valence band reduces the sub-surface electric field and hereby leads to flattening of the surface band bending. The flattening of the surface band bending induces lowering of the diamond work function. This is indeed detected in the KFM images as a higher (brighter) surface potential. The observed lowering of work function also corroborates the scheme of band bending at C-diamond surface (in the case of downward band bending the SPV effect would increase the work function).

In the case of PPy–diamond, a similar process as above takes place in the diamond part. Additionally, Frenkel excitons with strong binding energy are typically formed in conjugated polymers under illumination [29]. These excitons have to be dissociated to generate free holes. The diagram in Fig. 5 shows that the strongest potential slope for the exciton splitting is at the heterojunction of PPy with diamond. Because typical diffusion length of excitons in conjugated polymers (10 nm) is comparable to the PPy layer thickness (25 nm), excitons can easily reach the heterojunction. Nanoscale dimensions of PPy are thus crucial for effective exciton collection. Note that because of electric neutrality, excitons can travel freely through internal fields to the interfaces. Free holes are then most likely generated at the PPy–diamond heterojunction and consequently trapped in the diamond surface states. In these traps the holes can take part in the photo-excitation process into the diamond valence band.

The positive shift of surface potential in the case of PPy–diamond may correspond to an increase in surface band bending, i.e. to a depletion of holes near the PPy surface or interface. However, control experiments on the PPy–gold samples showed only a negligible response of PPy potential to illumination (presumably due to a high doping level achieved during electrochemical synthesis). This implies that by KFM we can "see" below PPy and observe SPV effects on the buried PPy–diamond interface [30]. Hence the SPV potential shift on PPy–diamond can be attributed mostly to this interface.

Smaller SPV shift of potential on PPy–diamond compared to shaved diamond may be due to several effects. First, absorption of light in PPy may reduce the light intensity passing to diamond. Second, transfer of holes from PPy to traps in diamond may partially compensate the SPV effect in diamond by increasing number of trapped holes in surface states. Third, charge transfer between PPy and diamond may occur, which results in a smaller potential difference between the components [31]. And last, energetic density of surface states may not be the same on nanoshaved and PPy–diamond. The KFM measurements alone cannot resolve these issues unambiguously. For instance comparing in-plane electronic transport measurements on PPy– and shaved diamond under variable illumination may shed more light on the actual mechanism. Such experiments are presently under way.

5. Conclusions

Thin layers of PPy were electrochemically attached to diamond surfaces and the opto-electronic properties of the resulting inorganic–organic heterosystem were characterized by KFM. As on the control sample (PPy–Au) the PPy films exhibited only negligible potential shifts (< 10 mV) under illumination, the potential differences were attributed to the surface photovoltage effects in the buried PPy–diamond interface. Such configuration allowed to establish the energetic model of PPy–diamond junction. The model suggests that: i) holes from initially surface-conductive diamond tend to be trapped in PPy trap states in thermal equilibrium under dark conditions, ii) excitons generated by super-band gap process in PPy split at the junction and the holes are trapped in diamond surface states. In what manner these holes contribute also to sub-band gap optical excitation of free holes in diamond depends on many factors (illumination, surface state density and occupation, etc.) and remains to be proved, for instance by electronic transport measurements. Yet the present data already indicate a charge transfer between PPy and diamond. SPV effects at the PPy–diamond interface may be thus promising for opto-electronic as well as bio-electronic applications due to nitrogen group within the PPy heterocycle.

Acknowledgments

We would like to acknowledge the kind assistance of Ing. V. Jurka with photolithography. This research was financially supported by projects KAN400100701 (GAAV), LC510 (MŠMT), LC06040 (MŠMT), 202/05/H003 (GAČR), AV0Z10100521, and by the Fellowship J.E. Purkyně.

References

[1] C.E. Nebel, Nature Mat. 2 (2003) 431.
[2] D. Shin, B. Rezek, N. Tokuda, D. Takeuchi, H. Watanabe, T. Nakamura, T. Yamamoto, C.E. Nebel, Phys. Status Solidi, A 203 (2006) 3245.
[3] M. Kalbacova, M. Kalbac, L. Dunsch, A. Kromka, M. Vanecek, B. Rezek, Phys. Status Solidi, B 11 (2007) 4356.
[4] A. Härtl, E. Schmich, J.A. Garrido, J. Hernando, S.C.R. Catharino, S. Walter, P. Feulner, A. Kromka, D. Steinmüller, M. Stutzmann, Nature Mat. 3 (2004) 736.
[5] J. Preclíková, F. Trojánek, B. Rezek, A. Kromka, B. Dzurňák, P. Malý, Phys. Status Solidi, A (in press), doi:10.1002/pssa.200879703.
[6] M. Liao, J. Alvarez, M. Imura, Y. Koide, Appl. Phys. Lett. 91 (2007) 163510.
[7] S. Koizumi, M. Kamo, Y. Sato, H. Ozaki, T. Inuzuka, Appl. Phys. Lett. 71 (1997) 1065.
[8] F. Maier, M. Riedel, B. Mantel, J. Ristein, L. Ley, Phys. Rev. Lett. 85 (2000) 3472.
[9] Z. Remeš, R. Petersen, K. Haenen, M. Nesládek, M. D'Oloeslaeger, Diam. Relat. Mater. 14 (2005) 556.
[10] D. Takeuchi, M. Riedel, J. Ristein, L. Ley, Phys. Rev., B 68 (2003) 041304 (R).
[11] H. Sirringhaus, N. Tessler, R. Friend, Science 280 (1998) 1741.
[12] B. Bolto, D. Weiss, Aust. J. Chem. 16 (1963) 1076.
[13] L. Micaroni, F. Nart, I. Hümmelgen, J. Solid State Electrochem. 7 (2002) 55.
[14] B. Rezek, D. Shin, T. Nakamura, C.E. Nebel, J. Am. Chem. Soc. 128 (2006) 3884.
[15] J. Mikat, I. Orgzall, H. Hochheimer, Phys. Rev., B 65 (2002) 174202.
[16] J. Lewis, K. Glaesemann, G. Voth, J. Fritsch, A.A. Demkov, J. Ortega, O. Sankey, Phys. Rev., B 64 (2001) 195103.
[17] P. Jelínek, H. Wang, J.P. Lewis, O.F. Sankey, J. Ortega, Phys. Rev., B 71 (2005) 235101.
[18] J. Čermák, B. Rezek, A. Kromka, M. Ledinský, J. Kočka, Diam. Relat. Mater. (submitted for publication).
[19] S.G. Ri, T. Mizumasa, Y. Akiba, Y. Hirose, T. Kurosu, M. Iida, Jpn. J. Appl. Phys. 34 (1995) 5550.
[20] B. Rezek, C.E. Nebel, Diam. Relat. Mater. 14 (2005) 466.
[21] W. Graupner, G. Leditzky, G. Leising, U. Scherf, Phys. Rev., B 54 (1996) 7610.
[22] P. Somani, S. Radhakrishnan, Chem. Phys. Lett. 379 (2003) 401.
[23] D. Takeuchi, C. Nebel, S. Yamasaki, Diam. Relat. Mater. 16 (2007) 823.
[24] F. Maier, J. Ristein, L. Ley, Phys. Rev., B 64 (2001) 65411.
[25] C. Saguy, E. Baskin, R. Kalish, Diam. Relat. Mater. 14 (2005) 344.
[26] L. Diederich, O.M. Küttel, P. Aebi, L. Schlapbach, Surf. Sci. 418 (1998) 219.
[27] B. Rezek, C.E. Nebel, M. Stutzmann, Diam Relat. Mater. 13 (2004) 740.
[28] C. Nebel, Semicond. Sci. Techol. 18 (2003) S1.
[29] K. Coakley, M. McGehee, Chem. Mater. 16 (2004) 4533.
[30] L. Kronik, Y. Shapira, Surf. Interface Anal. 31 (2001) 954.
[31] S.J. Wang, G. Cheng, X.H. Jiang, Y.C. Li, Y.B. Huang, Z.L. Du, Appl. Phys. Lett. 88 (2006) 212108.

4.5 In-plane electronic transport

The article "Illumination-induced charge transfer in polypyrrole-diamond nanosystem" *(J. Čermák et al., Diam. Relat. Mater. (2009)* ***18****, 800-803)* describes electric conductivity of a microscopic channel made on a diamond surface by selective hydrogen and oxygen termination. The channel is interrupted by electrochemically synthesized polypyrrole. In the dark the channel is electrically insulating. Under white light illumination the channel became electrically conductive. The conductivity is dependent on the illumination spectrum, being the most sensitive to blue wavelengths, which correlated well with the PPy absorption spectrum. Based on the energy band scheme and the surface photovoltage effect described in the previous article, we set up a model of doping of the diamond sub-surface region by holes from polypyrrole.

Diamond & Related Materials 18 (2009) 800–803

Contents lists available at ScienceDirect

Diamond & Related Materials

journal homepage: www.elsevier.com/locate/diamond

Illumination-induced charge transfer in polypyrrole–diamond nanosystem

J. Čermák *, A. Kromka, M. Ledinský, B. Rezek

Institute of Physics, ASCR, v.v.i., Cukrovarnická 10, 16200 Prague, Czech Republic

ARTICLE INFO

Available online 9 March 2009

Keywords:
Diamond
Polymers
Heterojunction
Electronic transport

ABSTRACT

Charge transfer in polypyrrole–diamond system is studied by conductivity measurements of a channel made of H-terminated diamond in the dark and under illumination. Micrometer-sized channels of conductive hydrogen-terminated diamond are lithographically fabricated on the surface of monocrystalline intrinsic diamond crystal by selective oxygen plasma treatment. The channels are interrupted by electrochemically synthesized micrometer-sized polypyrrole clusters. Similar characterizations are performed on channels interrupted by surface oxidation. Based on the increase and spectral response of the photo-current in the system, doping of diamond by charge carriers from polypyrrole is deduced.

1. Introduction

Diamond exhibits combination of unique properties such as high hardness [1], low chemical reactivity [2] or biocompatibility [3]. From the electronic point of view, diamond is a wide band gap (5.5 eV) inorganic semiconductor. Intrinsic diamond is thus electrically insulating and transparent for visible light. When the diamond surface is hydrogen-terminated (H-diamond), a thin (<10 nm) conductive layer is formed close to the diamond surface under ambient conditions [4]. These properties make it a promising semiconducting material for novel nanoscaled chemical and biological sensors [5] as well as for opto-electronic devices.

Other intensively studied materials for opto-electronic devices are conjugated polymers [6]. Their molecules can be easily modified to achieve specific properties like optical absorption or chemical reactivity. Polypyrrole (PPy) is one of the mostly studied examples. It can be synthesized by electropolymerization from aqueous solution of pyrrole (Py). When polymerized, conjugated chains are formed which are electrically and chemically stable with optical absorption in the visible region [7–9].

Combination of diamond with conjugated polymers is therefore a highly interesting system for diverse fields of applications. Transfer doping of diamond by fullerene molecules has been demonstrated [10], but electronic interaction between diamond and organic dyes such as PPy has not been studied yet. Recently, a charge transfer from covalently bound PPy to diamond has been indicated by Kelvin force microscopy [11], but the role of holes is still unclear.

In this paper we report on the influence of charge transfer between PPy molecules and diamond on the diamond surface conductivity. We show that photo-current in such system is greatly enhanced via the conjugated system of PPy. Influence of the photo-excited charge carriers in PPy on the electronic properties of diamond surface below is characterized by conductivity measurements in dark and under a visible light illumination. Illumination through color filters is used to resolve details of the charge transfer mechanism.

2. Experimental

Bulk monocrystalline intrinsic IIa (100) CVD diamonds (Element 6) were H-terminated in hydrogen microwave plasma (850 °C, 30 mbar, 1100 W) with resulting surface conductivity of 2×10^{-6}(S/□). Radio-frequency oxygen plasma (300 W, 3 min) treatment through a photo-lithographically patterned resin film was used to create electrically conductive micro-channels (5 μm wide) of H-diamond separated by O-diamond surface.

Au pads were thermally evaporated onto the channel ends to provide electrical contact. Thin layer of poly(methyl-methacrylate) (PMMA) was spin-coated in the thickness of 200 nm on the top of the diamond for encapsulation of electrical properties of the diamond surface. Rectangular openings (1×20 μm^2) in the PMMA layer were created by electron-beam lithography in the central part of the H-diamond micro-channel to specify the position of electrochemical synthesis. Schematic setup of the system is shown in Fig. 1a.

PPy was electrochemically deposited from solution of pyrrole (240 mM; Aldrich) and NaCl (100 mM) in deionized water. The electrochemical deposition was performed in galvanostatic regime with the constant current 400 nA supplied by a source-measure unit (Keithley) and with the H-diamond micro-channel employed as a working electrode. Platinum wire was used as a counter electrode. At such conditions, the applied voltage did not exceed 3.5 V. Subsequent characterizations were done after several (>5) hours after the deposition to ensure proper drying of PPy.

* Corresponding author. Tel.: +420 220 318 519; fax: +420 233 343 184.
E-mail address: cermakj@fzu.cz (J. Čermák).

0925-9635/$ – see front matter © 2009 Elsevier B.V. All rights reserved.
doi:10.1016/j.diamond.2009.02.031

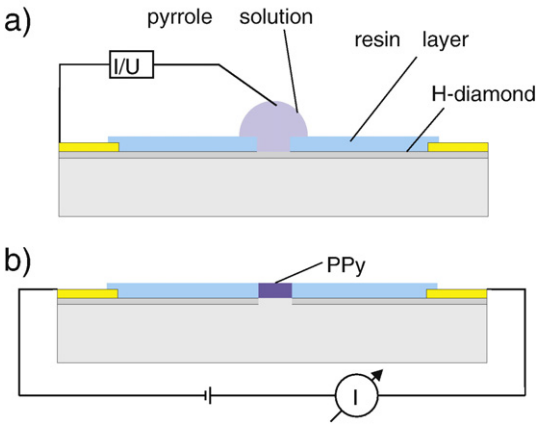

Fig. 1. Schematic experimental setup for a) PPy electrochemical synthesis and b) electric characterizations.

Electronic properties of the hybrid system were characterized by current–voltage (*I–V*) measurements in the instrument setup shown in the Fig. 1b. Measurements were performed both in the dark and under broad-band visible light illumination with tunable intensity (maximum illuminance: 40 klx). Spectral response of the system was studied by inserting color filters and tuning the light source intensity to achieve equivalent illuminance with all filters (approx. ten times lower illuminance than in the case of the broad-band visible light illumination). Similar characterizations were also performed on a H-diamond micro-channel without PPy cluster as well as on a micro-channel interrupted by oxidation of the surface in 1 μm wide region using oxygen plasma (parameters same as above for defining the channels).

Renishaw inVia Reflex Raman microscope (excitation wavelength 785 nm) was used to detect the formation of PPy on diamond. The diameter of focused excitation laser beam was 1 μm.

3. Results

Fig. 2 shows Raman spectra collected at the opening in the PMMA and its surrounding. Characteristic PPy maximum at 1600 cm^{-1} [12] proves the presence of PPy at the opening. Raman scattering maximum at 1332 cm^{-1}, which is attributed to diamond, was used for normalization of the spectra. Outside the active region only diamond signal is detected.

Fig. 3a shows *I–V* characteristics of the H-diamond micro-channels before the PPy deposition. They are linear, exhibiting resistivities of ~0.5 MΩ. Only negligible influence of illumination on the conductivities is observed. After the electrochemical deposition of PPy, the *I–V* characteristics changed significantly. In the dark, the channel becomes highly resistive as shown in Fig. 3b. Under a broad-band visible light illumination, the *I–V* characteristic becomes linear with a slope indicating mean resistivity of approx. 10 GΩ.

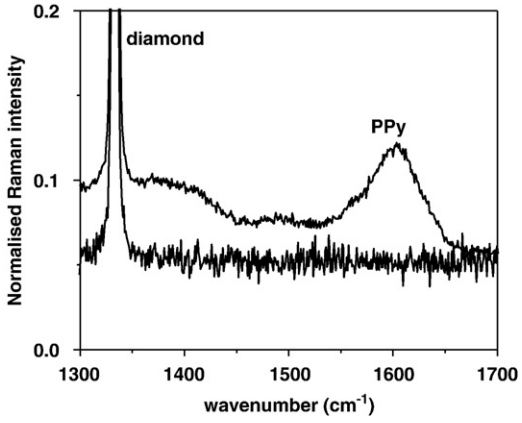

Fig. 2. Normalized micro-Raman scattering spectra out of the opening in the PMMA resin and at the PPy cluster showing typical PPy maximum at 1600 cm^{-1}. Maximum at 1332 cm^{-1} is attributed to diamond.

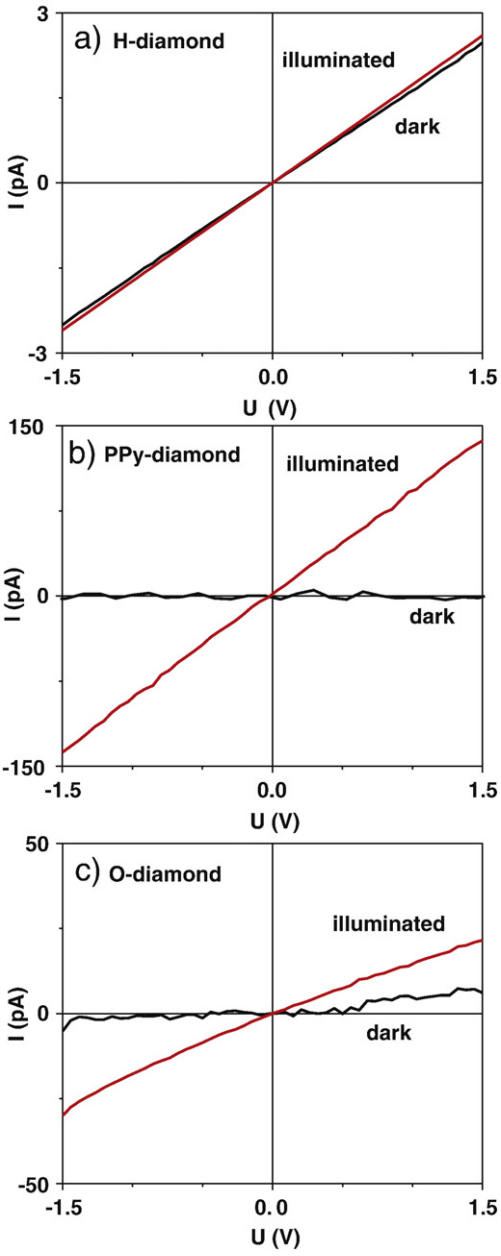

Fig. 3. Current–voltage characterizations in dark and under a broad-band visible light illumination of a) H-diamond, b) PPy-diamond and c) O-diamond.

Fig. 4a shows the current response to the periodic illumination on/off switching, when a constant bias voltage (1 V) is applied. The system reacts immediately (within 1 s) for both switching on and off and the current reaches repeatedly the same level. The current generated in diamond is also strongly dependent on the wavelength of the light, as shown in Fig. 4b. At the constant bias voltage (1 V), the detected currents under red, green, and blue illumination increase from around zero to 2 pA, 3 pA and 20 pA, respectively.

Fig. 3c shows that the micro-channel interrupted by surface oxidation is highly resistive in dark (200 GΩ) as well. Under illumination, the resistivity decreases to 75 GΩ. In the constant bias voltage regime (1 V) only low current changes (<5 pA) from around zero

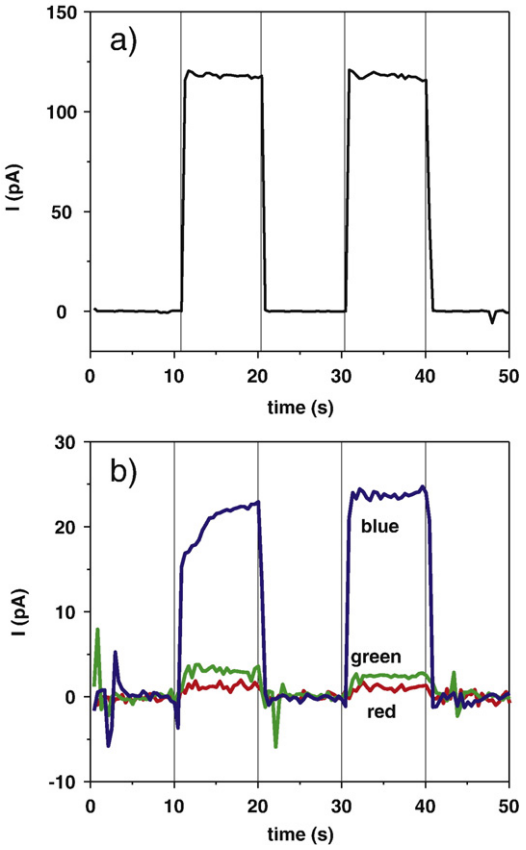

Fig. 4. Current as a function of time of PPy-diamond under repeated switching on and off of a a) broad-band visible light and b) spectrally resolved illumination under constant bias voltage 1 V applied. (For interpretation of the references to color in this figure legend, the reader is referred to the web version of this article.)

are observed under all types (red, green and blue) of illumination. No wavelength dependence could be detected at the applied light intensity.

4. Discussion

After the PPy deposition, the micro-channel becomes highly electrically resistive in the dark. Anodic oxidation of diamond surface during the electrochemical synthesis of PPy was minimized by the limiting the external voltage below 3.5 V. The actual potential at the electrically active area was further inherently reduced by the potential drop across the diamond surface due to its resistivity, potential drop on the Pt electrode (polarizing electrode), and potential drop across the electrolyte. So the actual potential directly at the interface is difficult to determine. To avoid these problems with various potential drops we have employed the galvanostatic regime. We don't claim though that there is no oxidation. Yet, if the surface oxidation was dominant, there would be hardly any PPy grafting on the surface as the surface would turn non-conductive beforehand. Therefore the loss of conductivity is attributed to the removal of H-termination while establishing covalent bonding of PPy to diamond [13]. We would also like to stress, that completely different nature of the surface treated by oxygen plasma and after PPy grafting was proved not only by the electrical properties (*I–V* characteristics) but also by different surface potentials detected by Kelvin probe microscopy on PPy-diamond and reference metallic samples [11] and by AFM nanoshaving experiments [13]. If the opto-electronic effects reported here were due to the oxidation, we would expect more pronounced opto-electronic effects on purely oxidized surface. That is not observed though. Larger surface conductivity and its strong spectral dependence on PPy-diamond compared to oxidized diamond further indicate that different phenomena are taking place and these systems are rather different. Therefore, in our opinion the surface oxidation plays only an insignificant role in the PPy grafting and observed opto-electronic phenomena.

Linear *I–V* characteristic observed on H-terminated micro-channels is common for the conductive H-diamond surface with Au contacts. *I–V* characteristics under illumination of both the channel interrupted by surface oxidation and the channel with PPy are also linear. This indicates similar transport mechanisms in both systems between PPy- or O-terminated diamond and H-diamond. Thus in both cases, the hole transport occurs obviously in valence band, as is well known for diamond surface conductivity [14].

A possible mechanism for this illumination-induced conductivity can be deduced based on the energetic schemes of PPy and diamond (Fig. 5). Intrinsic C-diamond is an insulating material. In equilibrium in dark, there are no free charge carriers to facilitate the charge transport. Simple model can be suggested based on the donor-like hole trap states located at energies 1.3–2.4 eV above the valence band maximum, which are reported for intrinsic C-diamond [15,16]. The Fermi level of C-diamond lies approximately at 2.3 eV above the valence band maximum in equilibrium [17], which is slightly higher than the trap states. Assuming positive electron affinity (up to 1.3 eV on reconstructed (100) C-diamond [18]) and typical diamond bandgap of 5.5 eV, the trap states are situated between around −5.2 eV below the vacuum level. Under illumination, holes from these trap states are excited to the valence band and a region with free charge carriers is created in the sub-surface area. The amount of the free charge carriers depends on the occupation of the trap states in the band gap and the light source wavelength and intensity. For C-diamond, the occupation of the trap states is very low due to the lack of charge carriers. The situation is similar to O-diamond surface and therefore the conductivity of C- or O-diamond is expected to be low under a sub-band gap (visible light) illumination. This is proved by the *I–V* measurements performed on the H-diamond channel interrupted by an O-diamond stripe.

Situation is different in the presence of PPy. PPy is a p-type semiconducting material with hole trap states at 0.1–0.4 eV above the HOMO [19]. The HOMO is reported to be situated at −5.0 eV with respect to vacuum level [20]. As a result, the trap states are situated between −4.6 and −4.9 eV with respect to vacuum level, which is

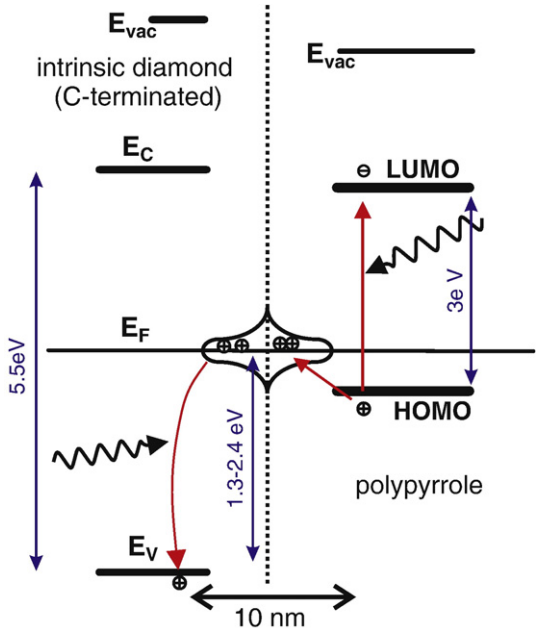

Fig. 5. Energetic scheme of the PPy-diamond system. Excitations in PPy supply charge carriers into the PPy trap states under illumination. The charge carriers are subsequently promoted to diamond surface states and photo-excited to its valence band.

almost the same as diamond's trap state energy level (Fig. 5). Excitons are generated in PPy under illumination by a super-band gap process. The most likely place for exciton splitting is at the PPy-diamond boundary [11]. As the energy positions of the trap states of PPy and C-diamond are similar, holes can move from PPy to C-diamond and increase the occupation of its band gap states. Such effect was observed by Kelvin force microscopy before [11]. The *I–V* measurements presented here show that these holes positively contribute to the photo-generation to valence band and hence increase the conductivity of diamond.

The above assertion is corroborated by the spectral response of the PPy-diamond system. Red light illumination (~1.7 eV) is energetic enough to excite charge carriers from diamond trap states to its valence band (~1.6 eV distance expected), but is not able to generate excitons in PPy (band gap around 2–3 eV [9,21]). Therefore the red light illumination is not able to significantly increase the conductivity of diamond. Green light illumination (~2.2 eV) starts generation of excitons in PPy and therefore the conductivity of the system is higher. Blue light illumination (~3.0 eV) is energetic enough to fully generate excitons in PPy [21] and the response of the system is the highest. Response of O-diamond at any spectral region was much lower (~3–5 pA). This is most likely due to the lack of free charge carriers in the trap states. Larger surface conductivity and its strong spectral dependence on PPy-diamond compared to oxidized diamond further indicate that different phenomena are taking place and these systems are rather different.

Other explanation of the increase of conductivity could be bridging of the gap in the conductive channel by PPy, which is in general a conductive material. However, high resistivity in the dark and the correlation with the surface photovoltage shifts (on PPy-diamond as well as on PPy-Au) reported before [11] are strong arguments against such possibility. Also the $I(V)$ curves would be most likely not linear because of H-diamond to PPy junction. Furthermore, charge transport in conjugated polymers is much more probable along the polymer chains than hopping to neighboring chains. Considering the experimental setup used for the electrochemical synthesis, the chains are oriented upright on the diamond surface. Therefore, lateral transport of charge carriers via PPy is most likely highly suppressed.

5. Conclusions

An order of magnitude larger conductivity of the diamond under PPy compared to oxidized diamond surface indicates transfer of charge carriers from PPy to diamond via exciton splitting. The observed charge transfer is crucial for development of novel devices for applications, where the combination of unique properties of diamond with the versatility of organic materials is needed. By choosing a specific conjugated polymer, devices based on this simple setup could cover wide range of chemical, biological or optical sensors. Moreover, the presence of covalent bonding between conjugated polymers and diamond makes such systems more stable and durable.

Acknowledgments

We would like to acknowledge a kind assistance of Ing. V. Jurka with electron-beam lithography and Dr. A. Fejfar for software development. This research was financially supported by projects KAN400100701 (GAAV), LC510 (MŠMT), LC06040 (MŠMT), 202/05/H003 (GAČR), AV0Z10100521, and by the Fellowship J.E. Purkyně (GAAV).

References

[1] C.E. Nebel, Nat. Matters 2 (2003) 431.
[2] D. Shin, B. Rezek, N. Tokuda, D. Takeuchi, H. Watanabe, T. Nakamura, T. Yamamoto, C. Nebel, Phys. Status Solidi, A Appl. Res. 203 (2006) 3245.
[3] M. Kalbáčová, M. Kalbáč, L. Dunsch, A. Kromka, M. Vaněček, B. Rezek, U. Hempel, S. Kmoch, Phys. Status Solidi, B Basic Res. 11 (2007) 4356.
[4] F. Maier, M. Riedel, B. Mantel, J. Ristein, L. Ley, Phys. Rev. Lett. 85 (2000) 3472.
[5] A. Härtl, E. Schmich, J.A. Garrido, J. Hernando, S.C.R. Catharino, S. Walter, P. Feulner, A. Kromka, D. Steinmüller, M. Stutzmann, Nat. Matters 3 (2004) 736.
[6] H. Sirringhaus, N. Tessler, R. Friend, Science 280 (1998) 1741.
[7] B. Bolto, D. Weiss, Aust. J. Chem. 16 (1963) 1076.
[8] R. Hamers, J. Butler, T. Lasseter, B. Nichols, J.R. Jr, K.-Y. Tse, W. Yang, Diamond Relat. Mater. 14 (2005) 661.
[9] L. Micaroni, F. Nart, I. Hümmelgen, J. Solid State Electrochem. 7 (2002) 55.
[10] P. Strobel, M. Riedel, J. Ristein, L. Ley, Nature 430 (2004) 439.
[11] B. Rezek, J. Čermák, A. Kromka, M. Ledinský, J. Kočka, Diamond Relat. Mater. 2–3 (2009) 249–252.
[12] J. Mikat, I. Orgzall, H. Hochheimer, Phys. Rev., B 65 (2002) 174202.
[13] J. Čermák, B. Rezek, A. Kromka, M. Ledinský, J. Kočka, Diamond Relat. Mater. (in press) doi:10.1016/j.diamond.2009.01.035.
[14] C. Nebel, B. Rezek, D. Shin, H. Watanabe, Phys. Status Solidi, A Appl. Res. 203 (2006) 3273.
[15] J. Ristein, Appl. Phys., A 82 (2006) 377.
[16] D. Takeuchi, C. Nebel, S. Yamasaki, Diamond Relat. Mater. 16 (2007) 823.
[17] C. Saguy, E. Baskin, R. Kalish, Diamond Relat. Mater. 14 (2005) 344.
[18] L. Diederich, O.M. Küttel, P. Aeby, L. Schlapbach, Surf. Sci. 418 (1998) 219.
[19] W. Graupner, G. Leditzky, G. Leising, U. Scherf, Phys. Rev., B 54 (1996) 7610.
[20] P. Somani, S. Radhakrishnan, Chem. Phys. Lett. 379 (2003) 401.
[21] J. Bredas, J. Scott, K. Yakushi, G. Street, Phys. Rev. B 30 (1984) 1023.

4.6 Hall mobility of holes

The article "Photo-conductivity and Hall mobility of holes at polypyrrole-diamond interface" *(J. Čermák et al., Diam. Relat. Mater. (2010)* ***19****, 174-177)* deals with Hall mobility measurement on polypyrrole-diamond system. We performed such an experiment to resolve the electric transport path as the reported charge carrier mobilities are very different (10^{-5}-10^{-10} cm^2/Vs for polypyrrole and 10^0-10^2 cm^2/Vs for diamond). We structured the surface of a monocrystalline diamond by selective oxygen and hydrogen termination to make it suitable for Hall mobility characterization. Polypyrrole was then electrochemically synthesized on it. The experiment was performed under the magnetic field 0.3 T and under intensive illumination (cold light source) in a well electrically shielded chamber. The detected Hall mobility of charge carriers in the system was 7±20 cm^2/Vs. Although the error bar of the resulting Hall mobility is relatively high, the obtained value is close to the expected mobility of charge carriers in diamond. The experiment thus independently supported our model of transfer of holes from polypyrrole to diamond under illumination.

Diamond & Related Materials 19 (2010) 174–177

Contents lists available at ScienceDirect

Diamond & Related Materials

journal homepage: www.elsevier.com/locate/diamond

Photo-conductivity and Hall mobility of holes at polypyrrole–diamond interface

J. Čermák *, B. Rezek, P. Hubík, J.J. Mareš, A. Kromka, A. Fejfar

Institute of Physics, Academy of Sciences of the Czech Republic, v.v.i., Cukrovarnická 10, 162 00, Prague 6, Czech Republic

ARTICLE INFO

Available online 30 September 2009

Keywords:
Diamond
Polypyrrole
Hall effect
Charge transfer
Charge carrier mobility

ABSTRACT

Surface of intrinsic monocrystalline diamoncd is selectively terminated by hydrogen and oxygen atoms to create electrically conductive microscopic square with contact leads in corners. Polypyrrole (PPy) film is then electrochemically deposited onto the H-terminated square. The resulting PPy-diamond system is characterized under a broad-band light illumination by four probe resistivity and Hall mobility measurements and the in-plane transport properties of holes at the PPy-diamond interface are evaluated. We also discuss applicability of these techniques on this specific heterosystem.

1. Introduction

Functionalization of diamond surfaces by organic molecules has recently attracted a lot of research effort as the combination of the unique diamond properties with the versatility of organic materials enables applicability in a wide range of innovative devices. A lot of work has been done in the development of diamond-based chemical [1,2] or biological [3–6] sensors. Functionalization of diamond surfaces by alkene, nitrophenyl [7] and especially by DNA [8,9] is also under intensive study. A linker molecule is usually needed to attach the active material to the diamond surface. Functionalization of diamond by organic molecules is pursued also for the so-called transfer doping of intrinsic diamond [10] as an alternative to H-termination of the surface [11] and for photovoltaic applications [2]. Properties of such hybrid diamond-organic systems are strongly influenced by the formation of covalent link, which cannot be established for all organics [6].

Polypyrrole (PPy) is an example of a conjugated polymer which can act as a biological linker due to the presence of amino-group in its main polymer chain. PPy can be synthesized on hydrogen-terminated diamond surface (H-diamond) electrochemically from an aqueous solution of pyrrole [12]. Polymerization forms conjugated chains which are electrically and chemically stable. Unlike some other conjugated polymers, PPy forms a covalent bond to diamond [12] which makes this system more stable. The optical absorption in visible region [13,14] and photo-sensitivity make PPy a promising material for opto-electronics as well [15].

Recently, charge transfer from PPy to diamond has been indicated by Kelvin force microscopy [16]. Further study of the conductivity and its dependence on the illumination spectral range showed that the holes transferred from PPy to diamond most likely give rise to the in-plane electric conductivity in the diamond subsurface area [17]. Nevertheless, alternative charge transport via PPy couldn't be excluded.

In this contribution we report on the possibility of direct identification of the transport path by measuring the charge carrier mobility as this quantity is a material specific property. In the case of PPy and diamond the identification is expected to be unambiguous as the characteristic charge carrier mobility differs by many orders of magnitude.

2. Experimental

Bulk monocrystalline intrinsic IIa (100) CVD diamond (Element 6) was H-terminated in hydrogen microwave plasma (850 °C, 30 mbar, 1100 W, 10 min). Radio-frequency oxygen plasma (300 W, 3 min) treatment through a photo-lithographically patterned resin film was used to create electrically conductive microscopic square ($10\times10\ \mu m^2$) with electric leads at the corners (Fig. 1a). Au contacts were thermally evaporated onto the leads. Resin film was spin-coated on the surface and a square opening ($13\times13\ \mu m^2$) rotated by 45° was prepared by UV lithography to restrict the active area for electrochemical deposition. PPy was synthesized according to the protocol in [12]. Specific parameters were: −50 nA (current density approximately 6 mA/cm^2), 150 s, counter electrode: platinum wire.

Sheet resistivity was measured in the van der Pauw configuration and differential electrometric arrangement (Fig. 2a), both in dark and under a broad-band light illumination (Schott KL2500; illuminance: 6×10^4 lx). Electric current (2 pA for measurement after the PPy deposition) was supplied by Keithley 220 source and the induced potential difference between the other electrodes was detected by two electrometers (Keithley 6514 and 237). The sample was mounted in a PTFE-based holder placed in a well shielded metallic chamber with a quartz window. Instruments were connected to the sample by triaxial cables with active guards to minimize cable charging and leakage currents.

* Corresponding author. Tel.: +420 220318519; fax: +420 233343184.
E-mail address: cermakj@fzu.cz (J. Čermák).

0925-9635/$ – see front matter © 2009 Elsevier B.V. All rights reserved.
doi:10.1016/j.diamond.2009.09.004

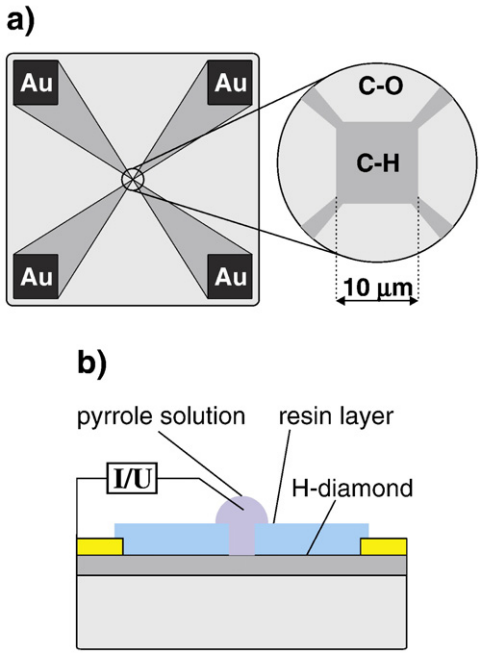

Fig. 1. a) Top view on the diamond C—H/C—O patterning b) schematic setup of the electrochemical synthesis of PPy on diamond.

Similar experimental setup was used also for the Hall mobility measurement with appropriate exchange of the connections (Fig. 2b). Magnetic field applied during this measurement was ± 0.3 T (H-diamond before PPy synthesis) and ± 0.2 T (after the PPy synthesis). Constant electric current was 2 pA. The Hall voltage was evaluated as an average of fifteen read-outs after thermal equilibration and RC relaxation. Measurement of small Hall voltages as differences of large potentials on voltage probes required sufficient time to reach an equilibrium after RC relaxation — typically 8–10 RC time constants of the measuring arrangement. As a result, one averaged Hall voltage value required approximately 30 min measurement time. All experiments were performed at room temperature.

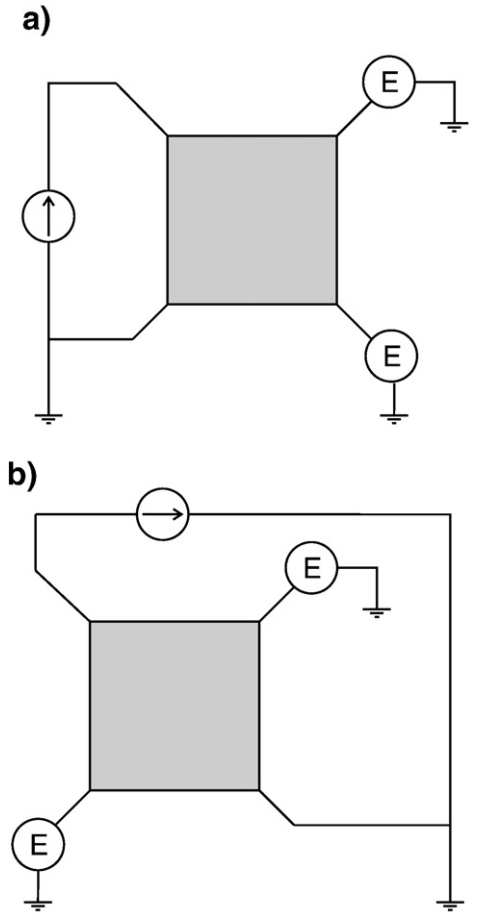

Fig. 2. Connection scheme for a) photo-conductivity b) Hall-mobility measurements.

3. Results

Sheet resistance of the H-diamond prior to PPy synthesis was 4.43×10^{3} Ω/□ with a surface charge carrier density 1.26×10^{13} cm^{-2}, both in dark and under illumination. Hall mobility of the diamond surface measured before the PPy synthesis was 112 ± 5 cm^2/Vs. The above values were similar in dark and under illumination.

After the electrochemical synthesis of PPy, the opening in the cover resin turned dark. The presence of PPy was proved by micro-Raman spectroscopy [12]. Fig. 3a shows the AFM topography image of the resulting PPy film after the resin removal. The height histogram in Fig. 3b shows that the PPy layer thickness is 80 ± 50 nm. The sheet resistance of the PPy-diamond system was higher than the detection limit in dark. Thus it was also not possible to determine the Hall mobility.

Under the illumination by the broad-band light from the top the sheet resistance of the PPy-diamond system decreased to 1.31×10^{12} Ω/□. Corresponding Hall voltage is plotted as a function of the magnetic field (±0.2 T) in the Fig. 4a. The Hall voltage was fluctuating within 8 mV range even though thermal stabilization and averaging were used at each value of magnetic field. The offset of the Hall voltage (22 mV) is most likely caused by the experimental setup (including sample asymmetry and/or inhomogeneity) and high resistivity of the system [18]. Nevertheless, if a linear fit is applied

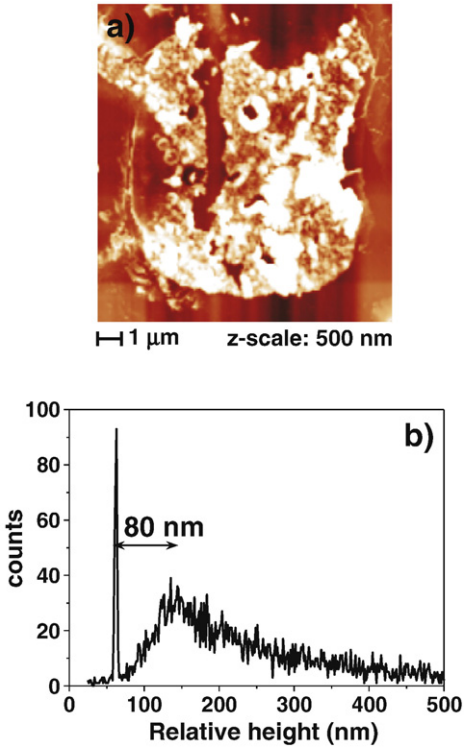

Fig. 3. a) AFM topography image of the synthesized PPy on diamond surface b) height histogram of the topography image.

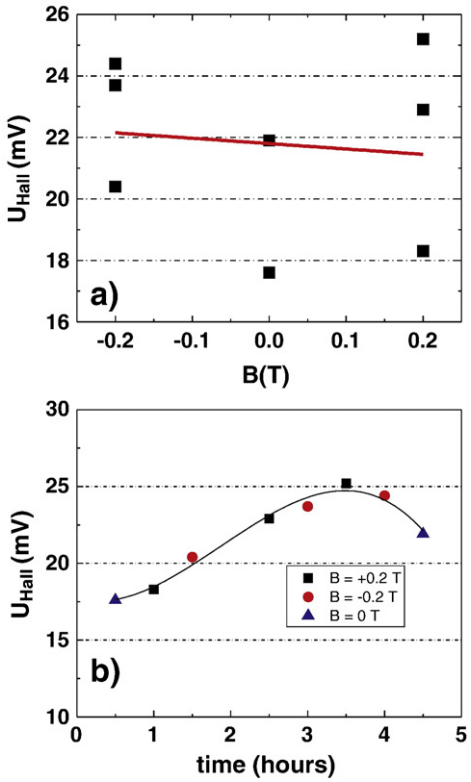

Fig. 4. a) Hall voltage as a function of magnetic field b) evolution of Hall voltage as a function of time.

and the offset is set to zero, the resulting Hall mobility of holes is 7 ± 20 cm^2/Vs.

The Hall voltage fluctuations appear less pronounced when the Hall voltage is plotted as a function of time, as shown in Fig. 4b. Obviously, there is a drift in the Hall voltage, which gives rise to the fluctuations when the Hall voltage is plotted as a function of magnetic field (Fig. 4a). The solid line in the Fig. 4b shows the approximation of the drift by a third degree polynomial. When this drift approximation is subtracted from the Hall voltage values the corrected mobility is 0.03 ± 6 cm^2/Vs.

4. Discussion

The measured mobility value can be used to resolve the transport path in the PPy-diamond system. If the path is all the way in diamond, the mobility should be in the same range as the mobility of H-terminated diamond surface, which is reported to be 10^0–10^2 cm^2/Vs [18]. If the charge transport takes place in PPy, the charge carrier mobility should be determined by the mobility in PPy. This value is strongly dependent on the synthesis method, substrate material or doping. Typical values of the charge carrier mobility in PPy are 10^{-5}–10^{-10} cm^2/Vs [19,20]. The highest reported mobility achieved by special doping using *p*-toluene sulfonate is 10^{-1} cm^2/Vs [21].

The relatively high error bar of the Hall mobility value reflects the instability of the detected Hall voltage values. As the instrumental setup was adjusted to minimize any external influence of the surrounding environment (grounded electrostatic shield, guarded triaxial cables, sufficient relaxation of the system before the measurement, averaging of multiple read-outs for each value) and to make such a small Hall voltage clearly detectable (high-sensitive electrometers in the differential arrangement), the instability must be originating in the PPy-diamond system itself. The Hall voltage values plotted as a function of time (Fig. 4b) supports this suggestion as it doesn't look like a random noise. Rather it follows a non-linear trend in time.

Part of this drift may be caused by the H-diamond leads that we use in our setup. Similar drift of Hall voltage on a pure H-diamond was already observed [18] and drift was attributed to the combined influence of environmental changes (as a surface effect, it is sensitive to the conditions close to it), capacitance effects in leads, and thermal equilibration.

Following the literature [18], we attempted to suppress the drift of the Hall voltages by subtracting a slow component as described above. The corrected Hall mobility, 0.03 ± 6 cm^2/Vs differs from the mobility achieved without correction (7 ± 20 cm^2/Vs). Such a change confirms that the measurement is significantly affected by the drift. It is probable that the approximation of the drift by a polynomial partially smoothes difference between Hall voltages belonging to the positive and negative magnetic fields. It leads to some underestimation of the evaluated mobility. Therefore the mean Hall mobility value lies most likely somewhere "in the middle" of the corrected and uncorrected values, i.e. at about 0.1–1 cm^2/Vs, however this cannot be concluded unambiguously. The upper estimate of the Hall mobility based on our measurements can be reliably given as 10–30 cm^2/Vs. The obtained value of mobility is thus in the range expected for the charge carrier transport in the diamond subsurface channel.

Reduction of the mobility with respect to the value measured before the PPy deposition can be explained by an enhanced hole scattering at PPy/diamond interface and/or reduction of the effective Hall mobility of the photogenerated holes due to surface recombination and low efficiency of their generation [22]. On the other hand, if the transport would occur in PPy the mobility should not be more than 10^{-5}–10^{-10} cm^2/Vs and most likely even less if we consider that the reported mobility in PPy is along the polymer chain, while in our case the PPy chains are mostly perpendicular to the charge transport direction [17]. Therefore, we believe that the above results give some, yet because of large measurement errors not full, support for the model of charge transport via diamond.

As follows from the above discussion, the time evolution of the Hall voltage makes the Hall mobility measurement extremely difficult, as the general limits of the technique are reached. Increasing the magnetic field or the electric current to induce higher Hall voltage differences would not help, as it would induce additional thermal effects. Therefore, another more suitable technique is needed to evaluate the charge carrier mobility more precisely. The major problem of the Hall effect technique, applied to high-resistive materials, is that it is too slow to cope with the drift. A possible technique which may be fast enough is the charge extraction in a linearly increasing voltage (CELIV) [23]. Experiments employing this technique are in preparation.

5. Conclusions

PPy was electrochemically synthesized on a diamond surface, which was patterned by oxygen and hydrogen termination into a microscopic shape suitable for photo-conductivity and Hall mobility measurements. Drifting of the Hall voltage originating likely in the PPy-diamond itself was observed. Upper estimate of the Hall mobility of 10–30 cm^2/Vs has been obtained, the mean mobility is in the order of 0.1–1 cm^2/Vs. It could not be measured exactly because of the drift. The above mobility values are compatible with the model of charge carrier transport via diamond, as suggested before by surface photovoltage measurements and in-plane current–voltage characteristics. Further suppression of the measurement errors in the Hall technique is limited because of the low system conductivity and significant Hall voltage drift. Faster technique is needed to avoid problems of drift and thus to enable determination of charge carrier mobility with better accuracy.

Acknowledgments

We would like to acknowledge Dr. Martin Ledinský for Raman spectroscopy measurements. This research was financially supported by projects KAN400100701 (AVČR), LC510 (MŠMT), LC06040 (MŠMT), 202/09/H041 (AVČR), AV0Z10100521, and by the Fellowship J.E. Purkyně (GAAV).

References

[1] B. Rezek, D. Shin, H. Watanabe, C. Nebel, Sens. Actuators, B, Chem. 122 (2007) 596.
[2] Y. Zhong, A. Midya, Z. Ng, Z.-K. Chen, M. Daenen, M. Nesladek, K.P. Loh, J. Am. Chem. Soc. 130 (2008) 17218.
[3] A. Härtl, E. Schmich, J.A. Garrido, J. Hernando, S.C.R. Catharino, S. Walter, P. Feulner, A. Kromka, D. Steinmüller, M. Stutzmann, Nat. Matters 3 (2004) 736.
[4] B. Rezek, L. Michalíková, E. Ukraintsev, A. Kromka, M. Kalbacova, Sensors 9 (2009) 3549.
[5] H. Gu, X. di Su, K.P. Loh, J. Phys. Chem., B 109 (2005) 13611.
[6] M. Stutzmann, J. Garrido, M. Eickhoff, M. Brandt, Phys. Status Solidi, A Appl. Res. 203 (2006) 3424.
[7] D. Shin, B. Rezek, N. Tokuda, D. Takeuchi, H. Watanabe, T. Nakamura, T. Yamamoto, C.E. Nebel, Phys. Status Solidi, A Appl. Res. 203 (2006) 3245.
[8] B. Rezek, D. Shin, T. Nakamura, C.E. Nebel, J. Am. Chem. Soc. 128 (2006) 3884.
[9] R. Hamers, J. Butler, T. Lasseter, B. Nichols, J.R. Jr., K.-Y. Tse, W. Yang, Diamond Relat. Mater. 14 (2005) 661–668.
[10] P. Strobel, M. Riedel, J. Ristein, L. Ley, Nature 430 (2004) 439.
[11] B. Rezek, C. Sauerer, C. Nebel, M. Stutzmann, Appl. Phys. Lett. 82 (2003) 2266.
[12] J. Čermák, B. Rezek, A. Kromka, M. Ledinský, J. Kočka, Diamond Relat. Mater. 18 (2009) 1098.
[13] B. Bolto, D. Weiss, Aust. J. Chem. 16 (1963) 1076.
[14] L. Micaroni, F. Nart, I. Hümmelgen, J. Solid State Electrochem. 7 (2002) 55.
[15] H. Sirringhaus, N. Tessler, R. Friend, Science 280 (1998) 1741.
[16] B. Rezek, J. Čermák, A. Kromka, M. Ledinský, J. Kočka, Diamond Relat. Mater. 18 (2009) 249.
[17] J. Čermák, A. Kromka, M. Ledinský, B. Rezek, Diamond Relat. Mater. 18 (2009) 800.
[18] O. Williams, R. Jackman, Semicond. Sci. Technol. 18 (2003) S34.
[19] R. Valaski, S. Ayoub, L. Micaroni, I. Hümmelgen, Thin Solid Films 415 (2002) 206.
[20] R. Valaski, S. Ayoub, L. Micaroni, I. Hümmelgen, Thin Solid Films 388 (2001) 171.
[21] K. Kanato, Thin Solid Films 393 (2001) 249.
[22] S.W. Edwards, T.H. Myers, J.F. Schetzina, Phys. Rev., B 21 (1980) 4697.
[23] G. Juška, K. Arlauskas, M. Viliunas, J. Kočka, Phys. Rev. Lett. 84 (2000) 4946.

Chapter 5

CONCLUSIONS

The thesis summarizes the results of various experimental techniques applied to two systems: fully organic heterostructures for photovoltaics, and diamond with electrochemically synthesized organic dye. Although these systems seem to be quite different, from the optoelectronic point of view they behave in a similar way. In both systems strongly bound excitons are created which dissociate at the interface with the other material.

Organic materials are expected to replace silicon at the dominant position in photovoltaics due to an easier fabrication processing and thus lower costs. The only barrier is their relatively low photovoltaic efficiency today. One approach how to improve the efficiency is a better control of microscopic morphology and opto-electronic properties. This needs proper characterization and evaluation with appropriate microscopic techniques.

We have contributed to this topic by several achievements. First we showed that the correlation of various advanced scanning probe techniques with micro-Raman mapping provides an universal and complex insight into the electronic properties of organic heterojunction films and may identify reasons for low photovoltaic efficiency. Second we used Kelvin force microscopy to study illumination induced shifts of surface potentials on organic blend thin films dynamically and locally. We also showed that adjusted advanced regimes of atomic force microscopy (Kelvin force microscopy, current-sensing atomic force microscopy) can reveal different opto-electronic properties of materials even if they look similar when the scanning regimes are performed in a standard way.

We demonstrated the applicability of the above methodology also to a hybrid organic-inorganic system. Systems consisting of diamond and organic materials are promising for various types of novel opto-electronic as well as biological or chemi-

cal sensors. To make such devices efficient, selective and reliable, basic electronic mechanisms at the diamond-organics interface have to be clarified. We intensively studied the electronic properties of an interface of a model polypyrrole-diamond system. We proved that during the electrochemical synthesis a covalent bond between diamond and polypyrrole is formed. Such finding is not achievable on all-carbon systems (polymer-diamond) by other common techniques such as X-ray photoelectron spectroscopy. Based on the advanced AFM characterization novel opto-electronic properties of this system were revealed. This motivated us to continue with further experiments, including spectrally resolved photocurrent and Hall mobility measurements. As a result a complex and well fitting model of charge transfer from polypyrrole to diamond under illumination via interfacial trap states was proposed. This model is supported by both indirect (loss of diamond surface conductivity after PPy deposition, surface photovoltage effect) and direct (Hall mobility measurement) experimental results.

The author's contribution

The author did all preparation steps of the samples under study including organic blend films spin-coating, multi-step optical lithography treatment, oxygen plasma discharge treatment, thermal evaporation of metals and electrochemical synthesis. The author performed all the atomic force microscopy experiments and subsequent data processing as well as macroscopic electronic characterization. The author gathered all additional experimental data and participated on their evaluation and interpretation. The author is the "corresponding author" and wrote the majority of the texts in the articles except for the article in the part 4 of Chapter 4. The article presented in the part 4 of Chapter 4 is based on experiments performed by the author and the author also significantly participated in the energy scheme construction, data interpretation and text preparation.

Bibliography

[1] B.A. Bolto, R. McNeill and D.E. Weiss. *Electronic conduction in polymers - III. electronic properties of polypyrrole.* Aust. J. Chem., **16**, 1090–1103 (1963).

[2] C.K. Chiang, Jr. C.R. Fincher, Y.W. Park, A.J. Heeger, H. Shirakawa, E.J. Louis, S.C. Gau and A.G. MacDiarmid. *Electrical Conductivity in Doped Polyacetylene.* Phys. rev. lett., **39**, 1098–1101 (1977).

[3] F. Garnier, A. Yassar R. Hajlaoui and P. Srivastava. *All-Polymer Field-Effect Transistor Realized by Printing Techniques.* Science, **265**, 1684–1686 (1994).

[4] T. Stübinger and W. Brütting. *Exciton diffusion and optical interference in organic donor-acceptor photovoltaic cells.* J. Appl. Phys., **90**, 3632–3641 (2001).

[5] S. Glenis, G. Tourillon and F. Garnier. *Influence of the doping on the photovoltaic properties of thin films of poly-3-methylthiophene.* Thin Solid Films, **139**, 221–231 (1968).

[6] S. Karg, W. Riess, V. Dyakonov and M. Schwoerer. *Electrical and optical characterization of poly(phenylene-vinylene) light emitting diodes.* Synthetic Metals, **54**, 427–433 (1993).

[7] G. Yu, J. Gao, J.C. Hummelen, F. Wudl and A.J. Heeger. *Polymer Photovoltaic Cells: Enhanced Efficiencies via a Network of Internal Donor-Acceptor Heterojunctions.* Science, **270**, 1789–1791 (1995).

[8] L.J.A. Koster, V.D. Mihailetchi and P.W.M. Blom. *Ultimate efficiency of polymer/fullerene bulk heterojunction solar cells.* Appl. Phys. Lett, **88**, 093511 (2006).

[9] W. Ma, C. Yang, X. Gong, K. Lee and A.J. Heeger. *Thermally stable, efficient polymer solar cells with nanoscale control of the interpenetrating network morphology.* Adv. Func. Mater., **15**, 1617 (2005).

[10] W. Ma, C. Yang, X. Gong, K. Lee and A.J. Heeger. *Thermally Stable, Efficient Polymer Solar Cells with Nanoscale Control of the Interpenetrating Network Morphology.* Adv. Func. Mater., **15**, 1617–1622 (2005).

[11] J. Peet, J.Y. Kim, N.E. Coates, W.L. Ma, D. Moses, A.J. Heeger and G.C. Bazan. *Efficiency enhancement in low-bandgap polymer solar cells by processing with alkane dithiols.* Nat. Mater., **6**, 497–500 (2007).

[12] J.Y. Kim, S.H. Kim, H.-H. Lee, K. Lee, W. Ma, X. Gong and A.J. Heeger. *New Architecture for High-Efficiency Polymer Photovoltaic Cells Using Solution-Based Titanium Oxide as an Optical Spacer.* Adv. Mater., **18**, 572–576 (2006).

[13] C. Soci, I.-W. Hwang, D. Moses, Z. Zhu, D. Waller, R. Gaudiana, Ch.J. Brabec and A.J. Heeger. *Photoconductivity of a Low-Bandgap Conjugated Polymer.* Adv. Func. Mater., **17**, 632–636 (2007).

[14] B. ÓRegan and M. Grätzel. *A low-cost, high-efficiency solar cell based on dye-sensitized collodial TiO_2 films.* Nature, **353**, 737 (1991).

[15] G. Binning, H. Rohrer, Ch. Gerber and E. Weibel. *Surface Studies by Scanning Tunneling Microscopy.* Phys. rev. lett., **49**, 57–61 (1982).

[16] G. Binning and C.F. Quate. *Atomic Force Microscope.* Phys. rev. lett., **56**, 930–933 (1986).

[17] B. Rezek, D. Shin, T. Nakamura and Ch.E. Nebel. *Geometric Properties of Covalently Bonded DNA on Single-Crystalline Diamond.* Diam. Relat. Mater., **128**, 3884–3885 (2006).

[18] Y-Sugimoto, P. Pou, M. Abe, P. Jelinek, R. Pérez, S. Morita and O. Custance. *Chemical identification of individual surface atoms by atomic force microscopy.* Nature, **446**, 64–67 (2007).

[19] M. Ledinský. *Optoelektronické a strukturní vlastnosti tenkých vrstev křemíku.* PhD thesis, Faculty of Mathematics and Physics, Charles University, Prague, Czech republic (2009).

[20] Z. Remeš, C. Uzan-Saguy, E. Baskin, R. Kalish, Y. Avigal, M. Nesladek and S. Koizumi. *Photo-Hall effect measurements in P, N and B-doped diamond at low temperatures.* Diam. Relat. Mater., **13**, 713–717 (2004).

[21] M. Riedel, J. Ristein and L. Ley. *Recovery of surface conductivity of H-terminated diamond after thermal annealing in vacuum.* Phys. rev. B, **69**, 125338 (2004).

[22] B. Rezek and C.E. Nebel. *Kelvin force microscopy on diamond surfaces and devices.* Diam. Relat. Mater., **14**, 466–469 (2005).

[23] B. Rezek, H. Watanabe, D. Shin, T. Yamamoto and C.E. Nebel. *Ion-sensitive field effect transistor on hydrogenated diamond.* Diam. Relat. Mater, **15**, 673–677 (2006).

[24] C.E. Nebel, B. Rezek, D. Shin and H. H. Watanabe. *Suraface electronic properties of H-terminated diamond in contact with adsorbates and electrolytes.* Phys. stat. sol. (a), **203**, 3273–3298 (2006).

[25] M. Amaral, A.G. Dias, P.S. Gomes, M.A. Lopes, R.F. Silva, J.D. Santos and M.H. Fernandes. *Nanocrystalline diamond: In vitro biocompatibility assessment by MG63 and human bone marrow cells cultures.* J. Biomed. Mater. Res. A, **87A**, 91–99 (2007).

[26] K.K. Kanazawa, A.F. Diaz, W.D. Gill, P.M. Grant, G.B. Street, G.P. Gardini and J.F. Kwak. *Polypyrrole: an electrochemically synthesized conducting organic polymer.* Synthetic Metals, **1**, 329–336 (1979/80).

[27] A. Mohammadi, M.A. Hasan, B. Liedberg, I. Lundström and W.R. Salaneck. *Chemical vapour deposition (CVD) of conducting polymers: polypyrrole.* Synthetic Metals, **14**, 189–197 (1986).

[28] S.V. Kasisomayajula, X. Qi, Ch. Vetter, K. Croes and D. Pavlacky. *A structural and morphological comparative study between chemically synthesized and photopolymerized poly(pyrrole).* J. Coat. Technol. Res., **7**, 145–158 (2010).

[29] M. Nakata and H. Kise. *Preparation of Polypyrrole-Poly(vinyl chloride) Composite Films by Interphase Oxidative Polymerization.* Polymer Journal, **25**, 91–94 (1993).

[30] M. Nakata, Y. Shiraishi, M. Taga and H. Kise. *Synthesis of electrically conductive polypyrrole films by interphase oxidative polymerization.* Makromolekulare chemie - macromolecular chemistry and physics, **193**, 765–771 (1992).

[31] L. Hong, Y. Li and C. M. Yang. *Fabrication and ammonia gas sensing of palladium/polypyrrole nanocomposite.* Sensors and Actuators B: Chemical, **145**, 25–31 (2010).

[32] X. Yang, L. Li and F. Yan. *Polypyrrole/silver composite nanotubes for gas sensors.* Sensors and Actuators B: Chemical, **145**, 495–500 (2010).

[33] A. Sun, Z. Li, T. Wei, Y. Li and P. Cui. *Highly sensitive humidity sensor at low humidity based on the quaternized polypyrrole composite film.* Sensors and Actuators B: Chemical, **142**, 197–203 (2009).

[34] A. Guiseppi-Elie. *Electroconductive hydrogels: Synthesis, characterization and biomedical applications.* Biomaterials, **31**, 2701–2716 (2010).

[35] M. Singh, P.K. Kathuroju and N. Jampana. *Polypyrrole based amperometric glucose biosensors.* Sensors and Actuators B: Chemical, **143**, 430–443 (2009).

[36] R.M.G. Rajapakse, K. Murakami, H.M.N. Bandara, R.M.M.Y. Rajapakse, K. Velauthamurti and S. Wijeratne. *Preparation and characterization of electronically conducting polypyrrole-montmorillonite nanocomposite and its potential application as a cathode material for oxygen reduction.* Electrochimica Acta, **55**, 2490–2497 (2010).

[37] Y. Yuan, S. Zhou and L. Zhuang. *Polypyrrole/carbon black composite as a novel oxygen reduction catalyst for microbial fuel cells.* Journal of Power Sources, **195**, 3490–3493 (2010).

[38] M. Selvaraj, S. Palraj, K. Maruthan, G. Rajagopal and G. Venkatachari. *Synthesis and Characterization of Polypyrrole Composites for Corrosion Protenction of Steel.* J. Appl. Pol. Sci., **116**, 1524–1537 (2010).

[39] G.J. Wang, L.C. Yang, Q.T. Qu, B. Wang, Y.P. Wu and R. Holze. *An aqueous rechargeable lithium battery based on doping and intercalation mechanisms.* J. Solid State Electrochem., **14**, 865–869 (2010).

Further extensive references are in the enclosed articles.

About the author

Curriculum Vitae

Personal data

Name:	Jan Čermák
Date of birth:	September 1981
Place of birth:	Prague
Nationality:	Czech
e-mail:	cermakj@fzu.cz

Education and research stays

June 2008	RNDr. degree obtained at the Faculty of Mathematics and Physics, Charles University in Prague.
June 2007	Research stay at Linz Institute for Organic Solar cells (LIOS), Johannes Kepler University, Linz, Austria; topic: preparation and characterization of blend organic thin films.
2006–present	Post-graduate studies at the Faculty of Mathematics and Physics, Charles University in Prague. (specialization: Optics and optoelectronics) Theme: *Organic-semiconductor interface study at nanoscale.*
June 2006	Mgr. degree obtained at the Charles University in Prague.
2001–2006	Graduate studies at the Faculty of Mathematics and Physics, Charles University in Prague. (specialization: Optics and optoelectronics) Theme: *New materials for solar cells.*

Research interests

Advanced AFM techniques for the characterization of surfaces of thin films.

Optoelectronic properties of diamond and its combination with organic dyes.

Languages

Czech, English, German (basic)

List of Publications

Impacted scientific journals

1. J. Čermák, B. Rezek, V. Cimrová, D. Výprachtický, M. Ledinský, T. Mates, A. Fejfar, J. Kočka, (2007), *Correlation of atomic force microscopy detecting local conductivity and micro-Raman spectroscopy on polymer-fullerene composite films*, Phys. Stat. Sol. rrl, 1, 193-195.

2. J. Čermák, A. Kromka, B. Rezek (2008), *Electrical characterization of locally charged oxidized nano-crystalline diamond films by Kelvin force microscopy*, Phys. Stat. Sol. a, 9, 2136-2140.

3. A. Kromka, Š. Potocký, J. Čermák, B. Rezek, J. Potměšil J. Zemek, M. Vaněček (2008), *Early stage of diamond growth at low temperature*, Diam. Relat. Mater. 17, 1252-1255.

4. B. Rezek, J. Čermák, A. Kromka, M. Ledinský, J. Kočka, (2009), *Photovoltage effects in polypyrrole-diamond nanosystem*, Diam. Relat. Mater. 18, 249-252.

5. J. Čermák, B. Rezek, A. Kromka, M. Ledinský, J. Kočka, (2009), *Electrochemical synthesis and electronic properties of polypyrrole on intrinsic diamond*, Diam. Relat. Mater., 18, 1098-1101.

6. J. Čermák, A. Kromka, M. Ledinský, B. Rezek (2009), *Illumination-induced charge transfer in polypyrrole-diamond nanosystem*, Diam. Relat. Mater. 18, 800-803.

7. J. Čermák, B. Rezek, V. Cimrová, D. Výprachtický, H.-H. Hörhold, M. Ledinský, A. Fejfar (2009), *Optoelectronic performance of poly(p-phenylenevinylene)-based heterostructures evaluated by scanning probe techniques*, Phys. Stat. Sol. b, 246, 2828-2831.

8. E. Verveniotis, J. Čermák, A. Kromka, B. Rezek (2009), *AFM induced electrostatic charging of nanocrystalline diamond on silicon*, Phys. Stat. Sol. b, 246, 2798-2801.

9. J. Čermák, B. Rezek, P. Hubík, J.J. Mareš, A. Kromka, A. Fejfar (2010), *Photoconductivity and Hall mobility of holes at polypyrrole-diamond interface*, Diam. Relat. Mater. 19, 174-177.

10. J. Čermák, B. Rezek, V. Cimrová, A. Fejfar, A. Purkrt, M. Vaněček, J. Kočka (2010), *Time-resolved opto-electronic properties of poly(3-hexylthiophene-2,5diyl)-fullerene heterostructures detected by Kelvin force microscopy*, Thin Solid Films, submitted.

Conference contributions and proceedings

1. J. Čermák, V. Cimrová, A. Fejfar: *Polyfluorene/polysilane - based solar cells*, poster and proceedings (editors: A. Fejfar, A. Vetushka), International Summer School: Science and Technology at Nanoscale, 6.-11.6. 2005, Tři Studně, Czech Republic.

2. J. Čermák, T. Mates, M. Ledinský, D. Výprachtický, V. Cimrová, A. Fejfar: *Studium tenkých organických vrstev pro sluneční články*, poster and proceedings, 2. česká fotovoltaická konference, 12.-14.6. 2006, Brno, Czech Republic.

3. J. Čermák, B. Rezek, V. Cimrová, M. Ledinský, T. Mates, A. Fejfar, J. Kočka: *Local Ordering and Optoelectronic Properties of Polymer-Fullerene Composite Films*, proceedings: VIII. Annual Linz Winter Workshop (Trauner Verlag, ISBN 978-3-85499-400-8, p. 37, editors: P. Hinterdorfer, G. Schütz, P. Pohl), 3.-6.2. 2007, Linz, Austria.

4. B. Rezek, J. Čermák, A. Kromka, M. Ledinský, A. Fejfar, J. Kočka: *Guided assembly of conjugated organic nanostructures on diamond and platinum films*, proceedings: VIII. Annual Linz Winter Workshop (Trauner Verlag, ISBN 978-3-85499-400-8, p. 1, editors: P. Hinterdorfer, G. Schütz, P. Pohl), 3.-6.2. 2007, Linz, Austria.

5. J. Čermák, B. Rezek, A. Kromka, M. Ledinský, A. Fejfar, J. Kočka: *Optoelectronic properties of polypyrrole-diamond nanostructures*, poster presentation: New Diamond and Nano Carbons, 28.-31.5. 2007, Osaka, Japan.

6. B. Rezek, J. Čermák, A. Kromka, M. Ledinský, A. Fejfar, J. Kočka: *Growth and properties of oriented polypyrrole nanowires on diamond*, poster presentation: New Diamond and Nano Carbons, 28.-31.5. 2007, Osaka, Japan.

7. M. Nesládek, P. Bergonzo, B. Rezek, J. Čermák, P. Hubík, J.J. Mareš, Y. Gregora: *Electrical transport in heavily B-doped diamond surface nanostructures*, oral presentation (M. Nesládek): New Diamond and Nano Carbons, 28.-31.5. 2007, Osaka, Japan.

8. J. Čermák, B. Rezek, A. Kromka, M. Ledinský, A. Fejfar, J. Kočka: *Optoelectronic properties of polypyrrole-diamond nanostructures*, oral presentation: Week od Doctoral Students 2007, 5.-7.6. 2007, Prague, Czech Republic.

9. A. Kromka, B. Rezek, Š. Potocký, J. Čermák, J. Potměšil, M. Vaněček: *Atomic force study of nanocrystalline diamond growth*, poster presentation; International Conference on Surfaces, Coatings and Nanostructured Materials - NanoSMat, 9.-11.7. 2007, Algarve, Portugal.

10. J. Čermák, V. Cimrová, D. Výprachtický, H.-H. Hörhold, A. Fejfar, M. Ledinský, J. Kočka: *Current-sensing AFM study of polymeric heterostructures*, poster presentation: Advanced polymer materials for photonics and electronics, 15.-19.7. 2007, Prague, Czech Republic.

11. J. Čermák, B. Rezek, V. Cimrová, D. Výprachtický, M. Ledinský, T. Mates, A. Fejfar, J. Kočka: *Correlation of current-sensing-AFM and micro-Raman spectroscopy on polymer-fullerene composites*, oral presentation: CU-NIMS Autumn School, 9.-12.10. 2007, Tsukuba, Japan.

12. J. Čermák, A. Kromka, B. Rezek: *Localized charging of oxidized nano-crystalline diamond surfaces by AFM tip*, poster, proceedings: Phys. Stat. Sol. a: SBDD XIII., 25.-27.2.2008, Hasselt, Belgium.

13. B. Rezek, J. Čermák, A. Kromka, M. Ledinský, J. Kočka: *Photovoltage effects in polypyrrole-diamond nanosystem*, oral presentation (B. Rezek) and proceedings in Diam. Relat. Mater.: New Diamond and Nano Carbons (NDNC2008), 26.-29.5.2008, Taipei, Taiwan.

14. J. Čermák, A. Kromka, B. Rezek: *Localized charging of oxidized nano-crystalline diamond surfaces by AFM tip*, poster (best poster award winner): Physics at Nanoscale, International Summer School, 16.-21.6.2008, Devět Skal, Czech Republic.

15. J. Čermák, B. Rezek, V. Cimrová, D. Výprachtický, H.-H. Hörhold, M. Ledinský, A. Fejfar: *Microscopic, optical and SPM techniques for organic devices enhancement*, poster: Seeing at the Nanoscale VI., 9.-11.7. 2008, Berlin, Deutschland.

16. J. Čermák, A. Kromka, B. Rezek: *Illumination-induced charge transfer in polypyrrole-diamond nanosystem*, oral presentation: Diamond 2008, 7.-11.9.2008, Sitges, Spain.

17. J. Čermák, B. Rezek, V. Cimrová, H.-H. Hörhold, M. Ledinský, A. Fejfar: *Characterization of structural and electronic properties of organic heterostructures by scanning probe techniques*, oral presentation and proceedings (ISBN: 978-80-254-3528-1, p. 28-33): 3. česká fotovoltaická konference, 3.-5.11. 2008, Brno, Czech Republic.

18. B. Rezek, J. Čermák, A. Kromka, M. Ledinský, J. Kočka: *Přenos náboje na rozhraní polypyrrolu a diamantu*, oral presentation and proceedings (ISBN: 978-80-254-3528-1, p. 70-76): 3. česká fotovoltaická konference, 3.-5.11. 2008, Brno, Czech Republic.

19. J. Čermák, B. Rezek, V. Cimrová, D. Výprachtický, H.-H. Hörhold, M. Ledinský, A. Fejfar: *Opto-electronic performance of PPV-based heterostructures evaluated by scanning probe techniques*, poster presentation, International Winterschool on Electronic Properties of Novel Materials, 7.-14.3. 2009, Kirchberg, Austria.

20. E. Verveniotis, J. Čermák, A. Kromka, B. Rezek: *AFM induced electrostatic charging of nanocrystalline diamond on silicon*, poster presentation, International Winterschool on Electronic Properties of Novel Materials, 7.-14.3. 2009, Kirchberg, Austria

21. J. Čermák, B. Rezek, P. Hubík, J.J. Mareš, A. Kromka, A. Fejfar: *In-plane Hole Transport in Polypyrrole-diamond Interface*, oral presentation and proceedings: Week of doctoral students, 2.-4.6. 2009, Prague, Czech republic.

22. E. Verveniotis, J. Čermák, A. Kromka, B. Rezek: *Local Electrostatic Charging on Semiconductor Thin Films*, oral presentation and proceedings: Week of doctoral students, 2.-4.6. 2009, Prague, Czech republic.

23. J. Čermák, B. Rezek, P. Hubík, J.J. Mareš, A. Kromka, A. Fejfar: *Photoconductivity and Hall mobility of holes at polypyrrole-diamond interface*, oral presentation and proceedings: New Diamond and Nano Carbons Conference 2009 (NDNC 2009), 7.-11.6. 2009, Traverse City, Michigan, USA.

24. J. Čermák, B. Rezek, V. Cimrová, A. Fejfar, A. Purkrt, M. Vaněček, J. Kočka: *Opto-electronic microscopic properties of organic heterostructures for photovoltaics*, oral presentation: International Conference on Amorphous and Nanocrystalline Semiconductors 2009 (ICANS 2009), 23.-28.8. 2009, Utrecht, Netherlands.

25. J. Čermák, B. Rezek, A. Kromka, M. Ledinský, A. Fejfar, P. Hubík, J.J. Mareš, J. Kočka: *Polypyrrole-diamond nanosystem synthesis and properties*, oral presentation and proceedings (ISBN: 978-80-254-5782-5, editors: B. Rezek, A. Kromka): Czech Workshop on Diamond Nanotechnology and Science (DINAS 2009), 5.-7.10.2009, Prague, Czech republic.

26. J. Čermák, B. Rezek, V. Cimrová, A. Fejfar: *Kelvin force microscopy on organic thin films*, oral presentation: Week of doctoral students, 1.-4.6. 2009, Prague, Czech republic.

27. E. Verveniotis, J. Čermák, A. Kromka, M. Ledinský, B. Rezek: *Electrostatic Charging Differences in Ultrathin Nanocrystalline Diamond*, oral presentation and proceedings: Week of doctoral students, 1.-4.6. 2009, Prague, Czech republic.

28. B. Stegemann, T. Lussky, A. Schöpke, J. Čermák, B. Rezek, J. Kočka, M. Schmidt: *Formation Kinetics and Charge Carrier Transport of Silicon Quantum Dot Layers*, oral presentation: 25th European Photovoltaic Solar Energy Conference and Exhibition, 6.-9.9.2010, Valencia, Spain.

Patents and patent applications

1. PV#2008-103: Způsob výroby elektrostaticky nabitých obrazců.
   international: WO 2009/106022: Method of making electrostatically charged patterns.

2. Patent No. 301547 (PV#2008-524): Způsob dopování diamantu přenosem náboje z organických barviv.
   international PCT/CZ2009/000104: Method of doping diamond using charge transfer from organic dyes.

Other achievements

1. Honorable mention in the Milan Odehnal Award for 2008 for the scientific work of young physicists organized by the Czech physical association, JČMF section.

2. Local conductivity image of a fullerene-polymer blend obtained by AFM microscope chosen for the 2008 Veeco calendar.

3. Winner of the Best poster award at the International Summer School on Physics at Nanoscale (Devět skal, Czech republic, 2008).